Available online at www.sciencedirect.com

ScienceDirect

Journal of Magnesium and Alloys 11 (2023) 4128–4145

www.elsevier.com/locate/jma

Review

Grain refinement and strength enhancement in Mg wrought alloys: A review

Sen Wang[a], Hucheng Pan[a,*], Dongsheng Xie[a], Dongdong Zhang[a], Jingren Li[b,*], Hongbo Xie[a], Yuping Ren[a], Gaowu Qin[a,*]

[a] *Key Laboratory for Anisotropy and Texture of Materials (Ministry of Education), College of Materials Science and Engineering, Northeastern University, Shenyang 110819, China*

[b] *Liaoning Academy of Materials, Institute of Materials Planification, Shenyang 110167, China*

Received 22 August 2023; received in revised form 3 November 2023; accepted 5 November 2023

Available online 29 November 2023

Abstract

Low absolute strength becomes one major obstacle for the wider applications of low/no rare-earth (RE) containing Mg alloys. This review firstly demonstrates the importance of grain refinement in improving strength of Mg alloys by comprehensively comparing with other strategy, e.g., precipitation strengthening. Dynamic recrystallization (DRX) plays a crucial role in refining grain size of Mg wrought alloys. Therefore, secondly, the DRX models, grain nucleation mechanisms and the related grain refinement abilities in Mg alloys are summarized, including phase boundary, twin boundary and general boundary induced recrystallization. Thirdly, the newly developed low-RE containing Mg alloy, e.g., Mg-Ce, Mg-Nd and Mg-Sm based alloys, and the RE-free Mg alloys, e.g., Mg-Al, Mg-Zn, Mg-Sn and Mg-Ca based alloy, are reviewed, with the focus on enhancing the mechanical properties mainly via the grain refinement strategy. At the last section, the perspectives and outstanding issues concerning high-performance Mg wrought alloys are also proposed. This review is meant to promote the deep understanding on the critical role of grain refinement in Mg alloys and provide reference for the development of other high strength and low-cost Mg alloys which are fabricated by the conventional extrusion/rolling processing.

Keywords: Magnesium alloy; Grain refinement; Strengthening; Dynamic recrystallization; Microstructure control.

1. Research background of wrought Mg alloys

Magnesium (Mg) alloy is commonly recognized as the lightest metallic structural materials [1–3]. Under the background of the continuous pushing on the "double carbon" target and also the urgent weight-saving demand for major equipment, Mg alloys have been considered as the critical materials, and have great opportunity to be used in the fields of aerospace, transportation and military [4–6]. However, the absolute strength of conventional Mg alloys is low, and their plasticity is poor due to the limited slipping system in the close-packed hexagonal structured matrix [7]. Therefore, developing Mg alloys with excellent mechanical properties such as strength and plasticity is one of the essential prerequisites for their service as structural materials. Previous studies have shown that precipitation strengthening (Mg-RE alloys [8–10]), grain refinement strengthening (extrusion, rolling, etc. [11–14]), and texture strengthening [15], are all beneficial for enhancing strength in wrought Mg alloys [15–18]. For example, the RE-containing Mg-6.8Y-2.5Zn (wt.%, $Mg_{97}Y_2Zn_1$ (at.%)) alloy processed via rapid solidification method has been reported to have yield strength exceeding 600 MPa [19]. More recently, the same $Mg_{97}Y_2Zn_1$ (at.%) alloy processed by ECAP and hot extrusion was prepared, exhibiting the high tensile yield stress of 475 MPa along with elongation of

* Corresponding authors.
E-mail addresses: panhc@atm.neu.edu.cn (H. Pan), jrli@lam.ln.cn (J. Li), qingw@smm.neu.edu.cn (G. Qin).

https://doi.org/10.1016/j.jma.2023.11.002

14.5% [20]. The highly-alloyed Mg-8.5Gd-2.3Y-1.8Ag-0.4Zr alloy also reaches an ultra-high strength of 575 MPa after rolling and following age-treatment [21]. Even at high temperature of 250 °C, the low alloyed Mg-RE alloys can reach 160 MPa [22]. In other words, the Mg alloys containing large amounts of heavy RE elements exhibit a good age-hardening response and can reach a high yield strength level (400 ∼ 600 MPa) [23–26]. However, the high cost of heavy RE elements and the scarcity of heavy RE resources (Gd, Ho, etc.), render the large-scaled usage of RE elements impossible in the wide industrial applications.

On the other hand, the Mg alloys containing non-RE elements of Zn, Sn and Al [27,28], and Mg alloys containing the light-RE elements of Nd, Sm and Ce [29,30], have also recently been developed. However, the non-RE/light-RE Mg alloys above usually exhibit low nucleation rate of the precipitated phases during the ageing treatment, and also the distribution of nano-phases are heterogeneous, which thus lead to the non-ideal strengthening effect. The rolling or extrusion process can effectively promote the dynamic precipitation of the nano-second phases and can simultaneously lead to grain refinement of the α-Mg matrix, which can contribute to the increased strength. The routine has been widely applied to many Mg alloying systems: Mg-Zn-Ca-Mn/Sm, Mg-Sn-Zn-Al/Nd, Mg-Zn-Ag-Ca-Zr and Mg-Al-Ca-Mn/Ce alloys [31–40]. However, the yield strengths of these non-RE/light-RE Mg alloys are yet less than 300 MPa, which cannot be comparable with those of the heavy-RE containing Mg alloys.

In fact, grain refinement is an important routine to increase the strength of Mg alloys, and the previous works have been focused on the severe plastic deformation (SPD) methods. The ultra-fined grains (< 1 μm) can be achieved in Mg alloys using SPD methods such as equal channel angular pressing [41–44] (ECAP), multi-directional forging [45–47] (MDF) and high pressure torsion [48,49] (HPT), and the yield strength of Mg alloys is thus significantly improved. For example, Ding et al. [50] obtained a high-strength AZ31 alloy (yield strength of 372 MPa and tensile strength of 445 MPa) using multi-pass ECAP. By controlling the deformation temperature and optimizing the path, the average grain size of AZ31 alloy can be refined to only 0.37 μm after 10 passes, which also has a strong basal texture, resulting in the ultra-high strength. Li et al. [51] fabricated Mg-1Ca alloys with a grain size of approximately 0.17 ± 0.52 μm by HPT, which increased the yield strength to 229.4 MPa, significantly higher than that of extruded Mg-1Ca alloys (∼ 130 MPa). Despite of that, the dimension of Mg samples produced by SPD routine is usually limited, which is insufficient for industrial applications. At the same time, Mg alloys fabricated by SPD methods are generally needed to be processed by several passes, thus bringing additional costs as compared with those of Al alloys. Considering this, manufacturing the high-performance Mg alloys with low/no RE content, i.e., low cost, and high strength-ductility synergy based on the conventional rapid extrusion and/or rolling process is now the key-point to further broaden their industrial applications.

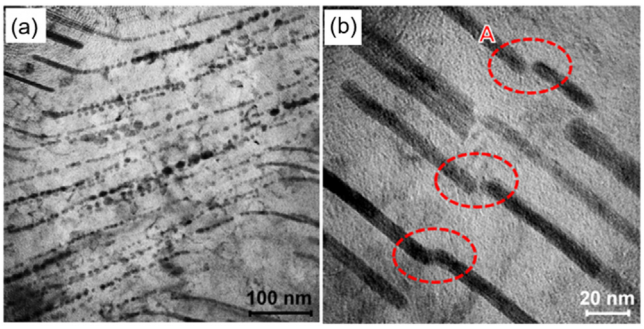

Fig. 1. (a) Morphology of the fractured precipitates in the severely deformed region of Mg-Zn alloy, (b) high magnification image showing the mechanisms of precipitate shearing by basal dislocations [67].

2. The importance of grain refinement for wrought Mg alloys

The bottleneck problem of current low-cost Mg wrought alloy is the insufficient absolute strength. Strengthening of Mg alloy can be achieved by introducing high density of the second phases, whereby age-hardening Mg alloying systems, including the Mg-Al-(Zn/Mn), Mg-RE(-Zn), Mg-Zn-(Zr) and Mg-Sn-(Zn/Al) alloys have been developed. However, the age-hardening effect of the above Mg alloys is not significant. For example, the precipitation strengthening contribution in the Mg-Al/Sn based alloys is only 30 ∼ 40 MPa [52–55], and the age-hardening value of Mg-Zn-(Zr) alloys with precipitation phases distributing on the prismatic plane can be slightly increased to 50 ∼ 70 MPa [56–59]. For the highly-alloyed Mg-RE-(Zn) based alloys, the age-hardening response is yet limited, only 140 ∼ 170 MPa [60–63]. It can be seen that there exists a large gap for the precipitation strengthening effect between Mg alloys (< 100 MPa) and Al alloys (300 ∼ 400 MPa [64–66]).

The mechanism for the above problem is that the typical strengthening phases in Mg alloys ($Mg_{17}Al_{12}$, β', etc.) can be easily cut through by dislocations, as evidence by the recent TEM examinations [67], so that the age-hardening effect of Mg alloys is not significant. For instance, LLorca et al. [67] performed micro pillar compression tests on an aged Mg-4Zn alloy, and found that the interactions between dislocations and precipitates during deformation contain more than just the dislocation bowing around the precipitates ($MgZn_2$, β_1',), but also the occurrence of precipitates shearing (Fig. 1). The dislocations shearing causes the fracture of the precipitated phase on the prismatic plane, and the shearing of β_1' phase can be ascribed to the fact that $(2\bar{1}\bar{1}0)$ plane of the β_1' phase has the highest atomic packing coefficient with the matrix of α-Mg. This was also confirmed by in situ TEM observations of the Mg-RE alloy by Huang et al. [68] and Bhattacharyya et al. [69]. The precipitate shearing on the prismatic plane has been observed in the WE43 alloy under the tension state, which is caused by basal slipping of $<a>$ dislocations, while the other non-basal <a> and $<c + a>$ dislocations cannot shear the precipitates. Ma et al. [70] directly observed that the basal

dislocation slipping can shear the LPSO phase with a high elastic modulus (75 ± 5 GPa) in Mg-Zn-Y alloy at the atomic level. The results show that even though the precipitates are located on the basal plane and have a high elastic modulus, the phases are still penetrated by many basal dislocations during deformation, which results in shearing. Besides, Wang et al. [71] further reported that pyramidal $<c + a>$ dislocations can shear the plate precipitates along pyramidal planes, when there is a good alignment between the slip plane of the incoming matrix dislocation and the pyramidal plane of precipitates. Otherwise, pyramidal $<c + a>$ dislocations sliding on matrix planes with low geometric compatibility with precipitates would bypass the nano-particles via Orowan looping mechanism.

A more detailed description of the shearing mechanism in the precipitates is investigated by molecular dynamics simulations by Esteban-Manzanares et al. [72]. The simulations show that the dislocations firstly enter the precipitates and form the Orowan loop nearby the precipitates. The appearance of new dislocations and the stress concentration associated with the dislocation pile-up eventually lead to the collapse of the Orowan loop and the precipitates shearing. By the way, experimental observations on precipitate shearing have also reported in the other Mg samples, including Mg-Nd [73], Mg-Mn-Nd [71] and Mg-Al [72,74] alloys. Consequently, second strengthening effect predicted by Orowan model should be overestimated considering only the case for precipitates shearing. Bhattacharyya et al. [69] obtained a strengthening value of 98 MPa for the precipitates in Mg-RE based on the Orowan bowing model, which is much higher than the experimental value of only 55 MPa. In other words, the precipitates in Mg alloys cannot effectively impede the slipping of <a> and/or $<c + a>$ dislocations, thereby resulting in the limited strengthening effects.

In contrast, the grain refinement strengthening in Mg alloys is particularly effective, as compared with second phase hardening (All refer to room temperature unless otherwise specified). Since Mg matrix is mainly deformed via dislocation slipping and twinning, the grain boundaries (GBs), as the atomic disorder regions, would impede the dislocation/twinning movement and create stress concentration in front of GBs, thus increasing the yield strength of the Mg alloy. According to the Hall-Petch relationship: $\sigma_y = \sigma_0 + kd^{-1/2}$, where σ_y is the yield stress, σ_0 is the friction stress, d is the average grain size, and k is the strengthening parameter, the above equation shows that grain size and strength are negatively correlated [75–77]. The slope k in the Hall-Petch relationship for Mg alloys can be as high as 200 ∼ 300 MPa $\mu m^{1/2}$ [78], which is 3 ∼ 5 times higher than the k value for Al alloys or steel (only 40 ∼ 70 MPa $\mu m^{1/2}$) [79]. For example, Huang et al. [80] prepared Al-0.3% Cu alloys with ultra-fine grains by cold rolling, and accurately quantified the contribution of boundary strengthening to flow stresses by excluding the dislocation strengthening and solid solution strengthening. By comparison with previous reports, it is shown that the Hall-Petch relationship for Al alloy can be extended from the micron- to the submicron-meter range with a slope k of approximately 45 MPa $\mu m^{1/2}$. For the Mg alloys, on the other hand, the k values for Mg-Al, Mg-Zn, Mg-Y and Mg-Gd alloys are fitted to 324, 322, 220 and 285 MPa $\mu m^{1/2}$, respectively [81]. Even though adding Gd and Y elements weakens the texture, resulting in extensive activation of both twinning and basal slip and thus decreasing the k values, they are still maintained above 200 MPa $\mu m^{1/2}$.

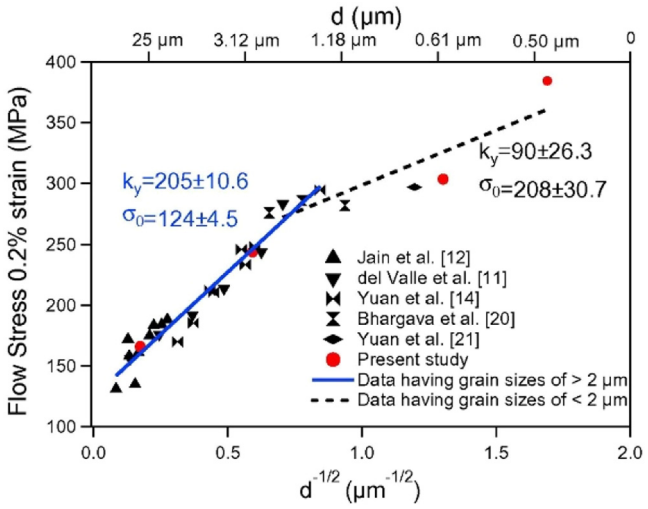

Fig. 2. Corresponding Hall–Petch (H-P) plot for prismatic slip including the data from the literature. One plot only includes the data for grain sizes >1 μm, the other plot consists of grain sizes down to 350 nm. k_y is the H-P slope [85].

In general, the Hall-Petch relationship can be applied for Mg alloys with grain sizes in the micron-meter range. When the grain size is refined to the nanometer level, a different Hall-Petch relationship slope can be obtained [82]. The change in k values is mainly attributed to a shift in the deformation mechanism caused by the variation in grain size. In metals with grain sizes at the microscale, dislocation or twin deformation mechanisms dominate the plastic deformation behavior; however, when grain sizes are reduced to the nanoscale, the deformation mechanism becomes associated with grain boundaries (e.g., grain boundaries sliding or creep) [83,84]. The k values corresponding to different grain sizes of AZ31 alloy have been studied by Razavi et al. [85]. As can be seen from the Fig. 2, the two regions corresponding to different k values are obtained, with k values of approximately 205 ± 10.6 MPa $\mu m^{1/2}$ when the grain size is greater than 2 μm, and k values of 90 ± 26.3 MPa $\mu m^{1/2}$ when the grain size is less than 2 μm. Statistical analysis of Mg-3Al-1Zn, Mg-9Al(−1Zn), and Mg-3Gd alloys by Zhang et al. [86] also showed that, regardless of the size of the grains used as the transition point, the k values of Mg alloys are yet much larger than those of Al alloys.

The refinement of grain size and thus the improvement of the strength in Mg alloys processed by various methods have been reported in many works [87–93]. For examples, the yield strength of AZ31 alloy increased from 244 MPa to

385 MPa when the grain size was refined from 2.9 μm to 0.3 μm, and an increase in strength of 141 MPa can be obtained [85]. The yield strength of AZ31 can be also increased by a factor of 2.65 when the grain size is refined from 75 μm to 2.5 μm through ECAP treatment, as reported by Lin et al. [94]. Pan et al. [95] obtained Mg-1.0Ca-1.0Al-0.2Zn-0.1Mn alloys with grain sizes in the range of 0.3 ∼ 0.6 μm after a simple extrusion treatment, which achieved an high yield strength of 425 MPa, accompanied by an elongation of 11%. The results above proved that the low/no-RE containing Mg alloys can be effectively strengthened via grain refinement.

3. Dynamic recrystallization and grain refinement of Mg alloys

Dynamic recrystallization (DRX) plays a crucial role in refining grain size during the plastic deformation of Mg alloys [96–98]. Previous studies have shown that during the low to mediate temperature forming process of pure Mg with low melting point, the activated dislocations mainly belong to the basal <a> and/or prismatic <a> type, with few occurrences of pyramidal $<c + a>$ slipping due to the high critical stresses [99,100]. In this sense, the migration rate of dislocation walls formed by the $<a>$-type dislocations recovery is quite fast because of the corresponding low critical resolved shear stress (CRSS) value, which leads to a rapid transformation from low angle grain boundaries (LAGBs) to high angle grain boundaries (HAGBs), thus offsetting most of the grain refinement effect. This is also one of the important reasons that it is difficult to obtain submicron sized grains Mg or Mg alloys (<1 μm) using traditional rolling or extrusion processes.

In order to fabricate the fined grains (< 10 μm) and/or ultra-fined grains (< 1 μm) in metals, the recrystallization process and controlling factors must be understood. It is widely accepted that DRX mechanism of metals is closely related to their stacking fault energy (SFE). For example, the low SFE of Cu undergoes discontinuous dynamic recrystallization (DDRX) mechanism which present clearly nucleation and growth stage, while the high SFE of Al tends to occur continuous dynamic recrystallization (CDRX) mechanism due to its easer cross slip capacity. The static dynamic recrystallization (SRX) mechanism during annealing after cold deformation is analogous, categorized as discontinuous static recrystallization (DSRX) mechanism and continuous static recrystallization (CSRX) mechanism. Great effort has been paid to study the recrystallization process from macro- to meso–scale, including the computer-aided microstructure simulation, which is benefited from improved computational methods and characterization technologies.

This section would sequentially introduce some typical simulation methods and the microstructural recrystallization mechanisms. We firstly separate simulation methods to two aspects: phenomenological model and computer-aided microstructural simulation. Then, the recrystallization mechanism according to the different recrystallization sites referring to the interface, such as phase boundary, special grain boundary (e. g., twin boundary) and general grain boundary are introduced, categorizing them by particle stimulated nucleation of recrystallization mechanism (PSN), deformation twinning induced nucleation of recrystallization mechanism (DTIN), and general grain boundary induced nucleation of recrystallization mechanism (GBIN), respectively.

3.1. Recrystallization simulation

3.1.1. Phenomenological constitutive model

Hot compression simulation was the earliest method to investigate the relationship between recrystallization process and the stress-strain correspondence. Arrhenius equation [101] is most widely used with the format of $\varepsilon = A(sinh\alpha\sigma)^n exp(-Q/RT)$, and this model is capable to simulate the stress-strain curves during hot compression at different temperature and strain rates by solving for the constants (A, α, n and Q) in the equation. Hu et al. [102] further implemented constitutive model into ABAQUS software, and found that it can simulate the measured force-displacement curves. Johnson-Cook model was proposed mainly to describe the deformation at high temperature and high strain rate. Compared with other models, this mode has received much attention due to its simple polynomial multiplication form ($\sigma = (A + B\varepsilon^n)(1 + C\ln\frac{\varepsilon}{\varepsilon_0})(1 - D(\frac{T-T_0}{T_m-T_0})^m)$($\varepsilon_0$: reference strain rate)), fewer solution parameters and more accurate prediction ability. Recently, Chen et al. [103] modified both the Arrhenius equation and Johson-Cook model in AZ80 alloy to more accurately match the flow stress curves. They found that Arrhenius type relation predicts the peak stress with high accuracy but cannot satisfy the strain relevant requirement while the Johnson-Cook model exhibits an inappropriate ability to describe the constitutive behavior. Further, the modified Arrhenius type relation is used to reflect the constitutive behavior before peak strain and the modified Johnson-Cook model can exhibit the stages after peak strain. Hollomon model [104] with the format of $\sigma = K\varepsilon^n\varepsilon^m$ can describe the sensitivity of materials to strain rates. Besides, there are also other constitutive models such as Ludwigson [105], Voce [106], KM[107], EM[108], Laasraoui-Janos[109], and Swift [110] model, which can be also used to predict the flow stress.

Based on the simulated macro stress-strain curve, phenomenological models for DRX simulations have also been developed. For example, the Zener-Hollomon parameter $Z = \varepsilon\exp(Q/RT)$ can be used to quantitatively analysis the DRX kinetics and DRXed grain size. Barezban et al. [111] found that the DRXed grain size can be expressed as $D = AZ^{-p}$ of Mg/Mg-0.5Gd/Mg-1.5Gd alloy with p value of −0.118, which is independent of the Gd content. Li et al. [112] obtained the relation of $D_{DRX} = 57.74 \cdot Z^{0.064}$ in a Mg-5.8Zn-0.5Zr-1.0Yb alloy. As regards the recrystallization kinetics, the widely used method is Johnson-Mehl-Avrami-Kalmogorav (JMAK) equation and presented as $X = 1 - \exp(-bt^n)$, which can predict the recrystallization fraction (Fig. 3) [112–114]. Nevertheless, it is noted that the phenomenological models mentioned above are all based on the macro stress-strain curves and constitutive

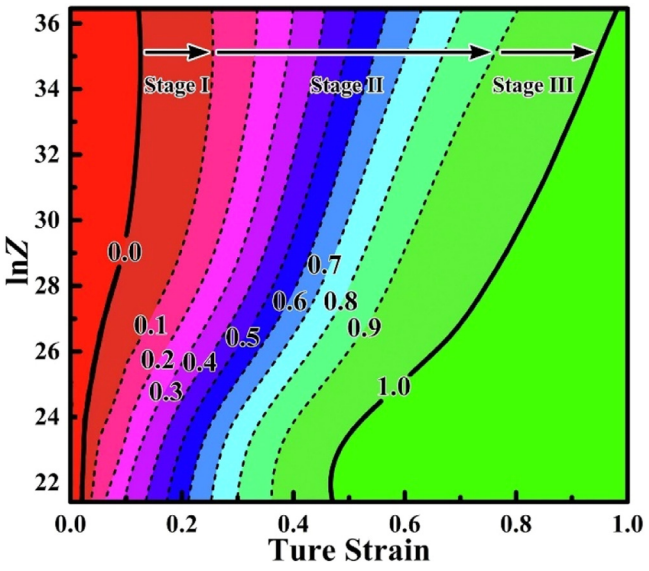

Fig. 3. The isofraction contour map of the parameter X_{DRX} to the relation among the Z parameter and ε [112].

theory which cannot directly reflect the microscopic deformation mechanism during the processing of Mg alloys and also always incapable to fully understand the detailed recrystallization mechanism.

3.1.2. Computer-aided microstructure simulation

Microstructure simulation is to analyze the micro-plastic deformation law of the polycrystalline under the applied external load based on the microscopic deformation mechanism, and then study the macroscopic plastic behavior of the material, which mainly including phase field (PF), cellular automata (CA), and Monte Carlo (MC) method. The above models can quantitatively reveal the microscopic deformation mechanism of the crystalline material, and thus establish the relationship between the microscopic deformation mechanism and the macroscopic mechanical behavior of the materials [115]. The greatest advantage of PF method is that there is a clear physical meaning since it is based on the Ginzburg-Landau theory. For example, Cai et al. [116] investigated the microstructure evolution and corresponding mechanical response based on the hot compression process by coupling PF-DDRX model and aforementioned phenomenological KM model, and the result is in good agreement with experimental data. They demonstrated that the developed model can quantitatively predict and design grain microstructures and mechanical properties. Recently, Song et al. [117] simulated the grain growth with second phase particles and applied stress during annealing process on industrial scale in a Y-alloyed ZK60 alloy by using phase field method. Their results revealed that there exists critical range of second particle size (0.3~0.4 μm) that can obtain the most refined grain size. Zhu et al. [118] further considered the pinning effect when particle size is refined and also considered the effect of second phase on the dislocation density evolution. As a result, their newly developed model exhibits great reliability and accuracy by inspecting the AZ80 alloy. Therefore, this model could be used to quantitatively predict the DRX behaviors in second phase containing Mg alloy, and could also be used to optimize the initial second phase morphology to obtain the desired microstructure. Popova et al. [119] integrated a CA model on the basis of a crystal plasticity finite element (FE) model, and calculated the evolution of the dislocation density during the material forming by the crystal plasticity model and analyzed the probability of the occurrence of recrystallization. The accuracy of the new method was also confirmed by studying the recrystallization data on a thin plate of AZ31 magnesium alloy. Duan et al. [120] investigated the dynamic recrystallization behavior of extruded AZ80A magnesium alloy during plastic deformation by coupling the physical-based FE method and the developed CA model. The established model was also embedded in DEFORM-3D software to simulate the grain evolution under various deformation conditions. This combined method was capable of predicting the evolution of flow stress, DRX volume fraction, and DRX grain size in various deformation conditions. He et al. [121] simulated the microstructure evolution of AZ31 Mg alloy at different temperatures and strain rates by using MC method. The results showed that high temperature is the main reason for grain growth, and increasing strain rate can promote recrystallization and refine grain size. Mohseni et al. [122] introduce pinning effect to MC method of the hot-rolled AZ61 Mg alloy, and successfully predicted the grain growth by comparing with experimental data. It is worth noting that even though all of the above models are able to simulate the DRX process, the specific DRX mechanism in the corresponding process yet cannot be revealed. In the following sections, the DRX mechanism based on the microstructure evolution, including the particle, dislocations, twins and grain boundaries would be reviewed.

3.2. Particle-stimulated nucleation of recrystallization (PSN)

During the thermomechanical processing, the DRX often occurs around isolated large particles (> 1 μm) in the matrix, and this phenomenon is called as the PSN. As early as 1994, Ball and Prangnell [123] investigated the recrystallization behavior of WE54 magnesium alloy, and firstly reported the recrystallization of PSN mechanism in Mg alloys. Xu et al. [124]. systematically studied the recrystallization behavior of AZ91 alloy and observed that the $Mg_{17}Al_{12}$ phase can cause the pinning effect, which prevent the recrystallized grains growth. They found that the conventional relationship between DRXed grain size and the Zener-Hollomon parameter ($Z = \varepsilon e^{\frac{Q}{RT}}$) would break down if the pinning effect of the precipitates is not fully considered. This indicates the importance of the PSN mechanism in refining grains, and the fine grains with the size of ~ 1.5 μm can be obtained under the $Mg_{17}Al_{12}$ pinning effect [125]. In the Mg-6.8Gd-4.5Y-1.1Nd-0.5Zr alloy, Xia et al. [126]. found the grain size can be refined from 200 μm to 27.2 μm when the strain increases to 1.61 at conditions of 500 °C and 0.5 s^{-1}, and suggested

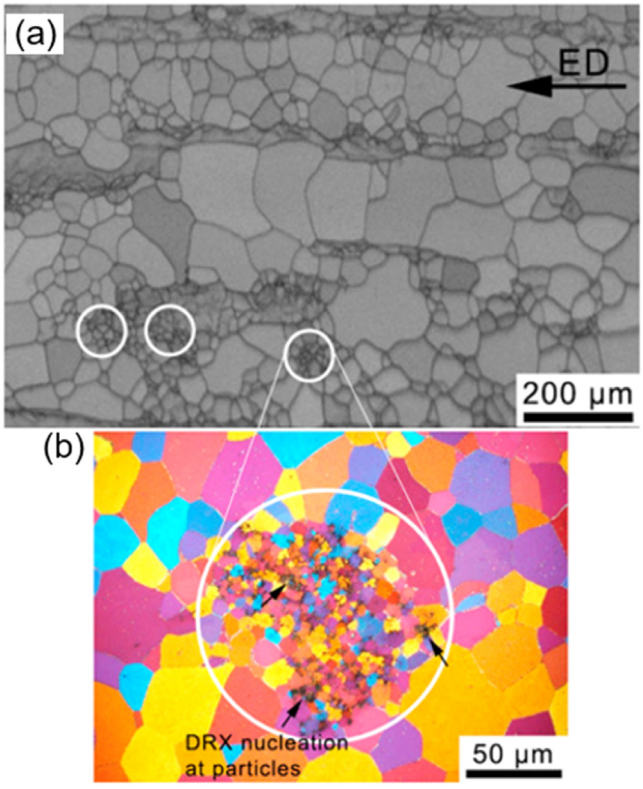

Fig. 4. EBSD band contrast microstructure of extruded ZWEK1000 magnesium alloy (a) and enlarged view of one fine grained area evincing particle-stimulated recrystallization [127].

that the second phase particles precipitated along the DRX grain boundaries play an important role in grain refinement.

In addition, Al-Samman et al. [127] performed a comparative experiments using Mg-1Zn-0.4Zr alloy without particles, and the RE-modified Mg-1Zn-0.4Zr alloy with 1 ∼ 10 μm particles. It is shown that the remarkble grain refining of ∼ 5 μm can be induced by particle stimulated nucleation, whereas the grain structure in the adjacent "particle-free" area is tremendously coarser (d ∼ 40 μm) (Fig. 4). Pei et al. [128] claimed that the coarse particle can served as particle stimulated nucleation site depending on clearly the locally stored dislocation density and the particle environment. Notably, Robson et al. [129]. conducted a PSN mechanism study on the model Mg-Mn binary alloys, and found that Mn particles greater than 1 μm can increase the strain gradient of the nearby Mg matrix during deformation, which is similar to the PSN mechanism in Al alloys [130]. The incompatible deformation between the second-phase particles and the Mg matrix would generate a high density of geometrically necessary dislocations and large orientation gradient around the hard particles, which can provide the necessary energy for DRX grains nucleation and growth. During annealing, the grains with size of ∼ 10 μm will be generated nearby the particles. Generally, the average size of DRX grains via PSN mechanism in Mg alloys would be larger than 1 μm, and other DRX mechanisms should be incorporated.

3.3. Deformation twinning induced nucleation of recrystallization (DTIN)

Besides the DRX at phase boundaries (PSN mechanism), twin boundaries can also serve as the nucleation site for recrystallization, especially the compression twin boundary with limited mobility. Generally, three typical DRX sites have been reported in regard to the DTIN mechanism, including the twin interiors, twin–twin intersection and twin–GB intersection.

Firstly, the recrystallization can readily occur in the twin interiors due to the dislocation concentration. For the tension twins, the internal strain can be easily released due to the high twin boundary mobility, which would not lead to high strain accumulation. On the other hand, for the compression twins formed at the later stage of deformation, the dislocations would gradually accumulate around the twin boundary, which also lead to the inhomogeneous lattice strain in the twin interiors. These localized deformation areas can easily serve as the nucleation sites for DRX, which also act as an effective softening mechanism. Particularly, the previous works have showed that the DRX behaviors at the twin interiors are determined by the twin types and twin generation. For example, Li et al. [131] investigated the early stage static recrystallization process of the AZ31 extruded plate, and found that recrystallization mainly arise from the compression twins, rather than extension twins, and the orientations of new DRX grains are close to those of the twin matrix. The recrystallization grain size is limited to 1 ∼ 3 μm since the thickness of formed compression twin is only 3 ∼ 5 μm. Furthermore, Basu et al. [132] studied the recrystallization mechanism of Mg-1Gd and Mg-1Ce alloys, and found that both the compression twin and double twin interior regions can be recrystallized during hot compression process. The newly formed grains' orientation is also close to twined grain's orientation, and the misorientation between new DRX grains is low at the early stage of recrystallization. Besides, the recrystallization inside compression twin and double twin can effectively refine the initial parent grains size by 1 ∼ 2 orders of magnitude, ∼ 10 μm in size. Guan et al. [133] further studied the effect of twin on the recrystallization behavior of WE43 magnesium alloy, and the quasi-in-situ EBSD results indicate that the preferential nucleation site for recrystallization was $\{10\bar{1}1\}$–$\{10\bar{1}2\}$ double twins (DTWs) interiors, and the recrystallized grains can be decreased from ∼ 200 μm to ∼ 70 μm.

Secondly, when recrystallization nucleation site is at the compression twin–twin intersections, the orientation of the new grain is more random and the grain size can be also refined due to the DRX process. For example, Li et al. [131] investigated the case of recrystallization from intersection of two compression twin bands, and the experimental results indicate that DRXed grains with a spread spectrum of orientation up to 90° away from original twinned matrix, and with size of 1 ∼ 3 μm (Fig. 5). Thirdly, when the recrystallization nucleation site are at compression twin–GB intersections, the newly formed grains' orientation are also random. Guan et al. [133] reported that the most recrystallized grains were from DTWs and also DTW–GB intersections. During subse-

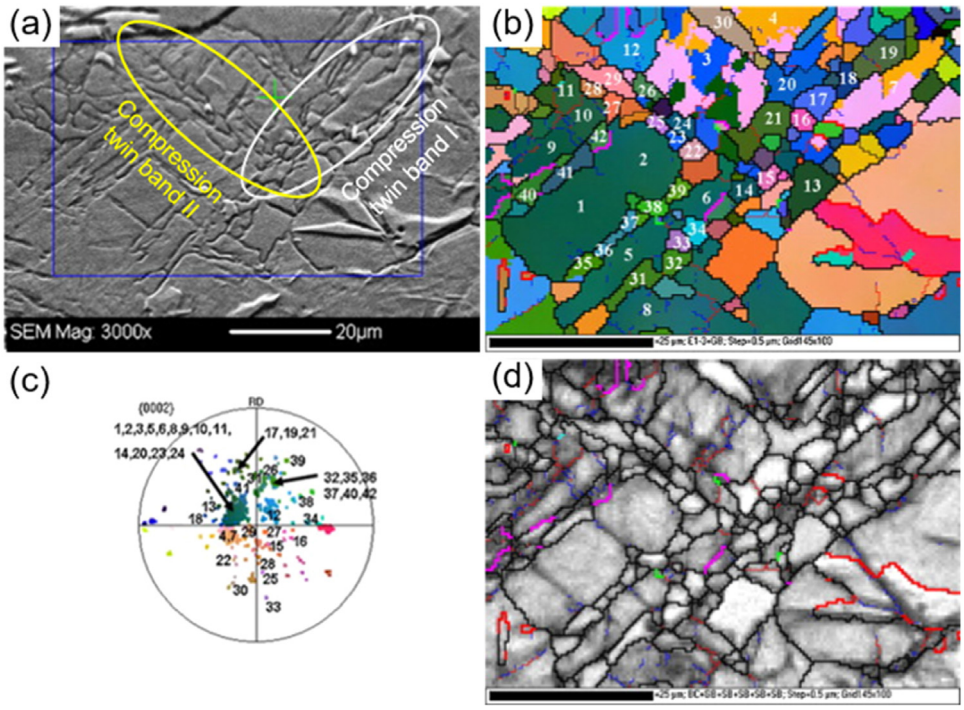

Fig. 5. Orientatin map of nucleation at two compression twin bands (a) micrograph (b) orientation map (c) (0002) pole figure (d) Kikuchi band quality [131].

quent growth, the recrystallized grains within the individual DTW lamellae are constrained and are even consumed by the other recrystallized grains. Moreover, the recrystallized grains originating from DTW–DTW and DTW–GB intersections can readily grow into the deformed parent grains and subsequently into the neighboring deformed grains, i.e., the regions with higher stored energy (Fig. 6).

By the way, shear bands can act as the additional sites for nucleation of DRX grains in Mg alloys. In plastically deformed alloys, shear bands are narrow regions involving severe plastic deformation [134]. In Mg alloys, shear bands are generally composed of compression twin and double twin arrays, as well as a large number of dislocations. Zeng et al. [135] reported that in cold rolled Mg-0.3Zn-0.1Ca alloy, shear bands induced recrystallization occurred at the beginning of annealing treatment, which is similar with the DRX nucleation at twin sites above. For the texture intensity and texture type of recrystallization grains origination from shear band, there still exist some controversy viewpoints. The "RE-texture" was first proposed in some low alloyed extrusion Mg-RE binary alloys by Stanford [136], and the "RE-texture" grains are found to nucleated at the shear bands with an angle deviation of ~ 35° from extrusion direction. Guan et al. [137] also reported that the shear bands can be the preferential recrystallization sites but they claimed that shear band nucleation contribute little to the RE-texture component. Further works are yet needed to clarify the role of shear bands on DRX process in Mg alloys. Besides, the grain refinement effect by shear bands is similar to that of compression twins and double twins. It is concluded that the average size of DRX grains formed via TSIN mechanism in Mg alloys would be larger than 1 μm, frequently even larger than 10 μm.

3.4. General grain boundary induced nucleation of recrystallization (GBIN)

Besides the recrystallization sites at phase boundary and twin boundary, general grain boundary can also act as the recrystallization site due to the dislocation accumulations at the grain boundary. For example, Jiang et al. [138] found that during the extrusion of a AZ31 alloy there is no obvious evidence showing the DRX nucleation at twinning and/or particles, but the occurrence of nucleation at GBs are found due to severer lattice rotations around the GBs and thus LAGBs or sub-grains are gradually formed. At the microscale, the formation of new grains in Mg alloys occurs mainly via the dislocation activation, movement and rearrangement. Imandoust et al. [139] noted that during CDRX of Mg alloys, basal $<a>$/pyramidal $<c + a>$ dislocations can accumulate to form the basal-typed LAGBs (parallel to basal plane) and/or the prismatic-typed LAGBs (parallel to prismatic plane), while the prismatic $<a>$ dislocations can only rearrange to form the prismatic-typed LAGBs. The formed LAGBs can continue to absorb dislocations and gradually evolve into the HAGBs in the subsequent recrystallization process. The results indicate that new grains formed via the CDRX mechanism in Mg-0.51Ce alloy are usually < 5 μm in size, despite that the deformation temperature is as high as ~ 450 °C (Fig. 7). On the other hand, when DDRX occurs in Mg alloys, recrystallization originates from the aggregated

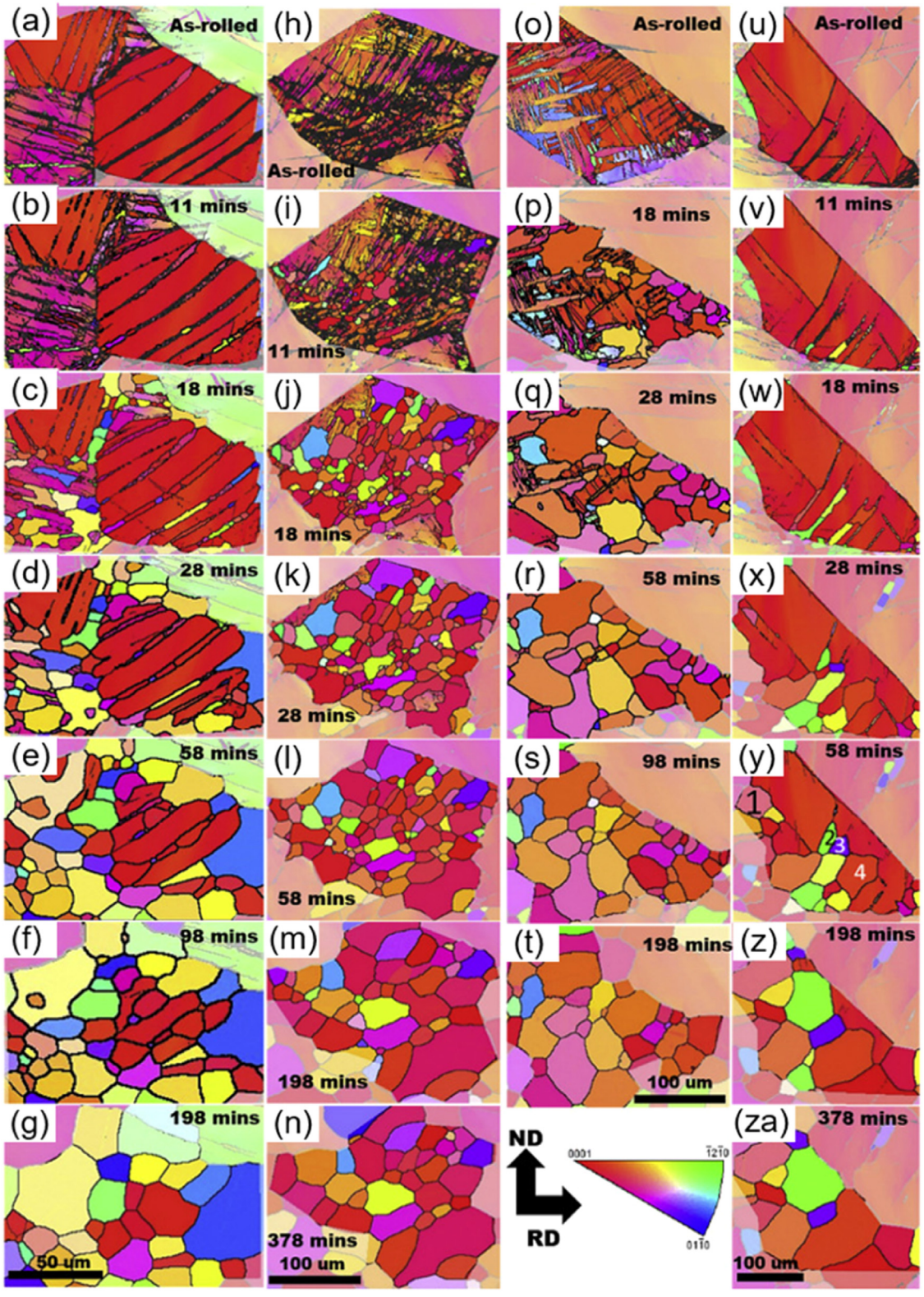

Fig. 6. Quasi-in-situ EBSD IPF maps superimposed by band contrast maps displaying evolution of twins in individual grains annealed at 490 °C with various times (a-g) DTW, (h-n) DTW, TTW–TTW, (o-t) DTW, TTW, TTW–TTW and (u-za) DTW–GB intersections [133].

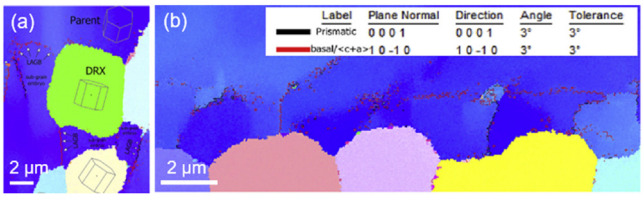

Fig. 7. (a) EBSD results of Mg-0.51 wt% Ce extruded alloy presented relaxation of basal/$<c+a>$ (red lines) and prismatic dislocations (black lines). (b) concomitant relaxation of basal/$<c+a>$ and prismatic dislocations at CDRX front [139].

dislocations around the original HAGBs. Imandoust et al. [140] considered that a dislocation density gradient can be formed from the grain boundaries to the grain interiors due to the dislocations aggregate. Consequently, recrystallized grains are formed through the grain boundary bow out mechanism. The newly developed recrystallized grains exhibit a "necklace like" distribution, with recrystallized grain sizes ranging from 5 to 10 μm. Another work on Mg-1.10Zn-0.49Al-0.30Mn-2.2Y-0.41MM (misch metal) wt.% also show that the new grains formed via DDRX mechanism is usually < 10 μm in size, when the deformation temperature is ~ 450 °C.

In addition, the solute segregation can also modify the average size and orientation of DRX grains to some certain extents. In conventional Mg alloys, there exists a preferred selection of crystal orientation during nucleation and growth of dynamically recrystallized grains, either $<11\bar{2}0>$ axis or the $<10\bar{1}0>$ axis being parallel with the extrusion direction. The extrusion $<10\bar{1}0>\|$ED texture can always transform to $<10\bar{1}0>-<11\bar{2}0>\|$ED texture component by subsequent annealing or continuous deformation. Barrett et al. [141] reported that the experimental-observed $\{13\bar{4}0\}$ boundary is associated with the texture transformation, which is also known as Σ13 boundary with 30° <0001> misorientation between the two textured grains above. The further simulation results show that the $\{13\bar{4}0\}$ boundary has a minimum local energy, which will be preferentially formed during the recrystallization process. However, after the addition of RE elements which can easily migrate to the GBs, the other general GBs energy can be remarkably decreased, which is even comparable with that of the $\{13\bar{4}0\}$ GB [142]. Consequently, the preferential 30° <0001> transformation would be suppressed, and the other ordinary GBs would have more opportunity for growth, which thus lead to the fiber textures randomization.

Further, the solute segregation not only decorates the recrystallization texture but also limit the growth of recrystallized grains. It is known that the tendency of solute segregation at grain boundaries is strongly associated with the type of solute elements in Mg alloys. Ordinarily, RE [143], Ca [135], Zn [144], and Ag elements [145] have been confirmed to segregate at grain boundaries, which should be due to the large segregation energy [142,146]. For example, Zhang et al. [147] obtained grain size of ~ 6.9 μm in a Mg-2Er alloy extruded at 320 °C. After the subsequent annealing at 300 °C for 1 h, the fully recrystallized grains remain fine grain size of ~ 8.3 μm due to the segregation of Er atoms at grain boundaries. Pan et al. [148,149] reported that extruded Mg-Sn-Ca-(Mn) alloys can refine to only ~ 320 μm due to the Ca segregation at LAGBs and dislocations. Xiao et al. [145] found that Ag segregation can refine the grain size of Mg matrix to only ~ 105 nm (Fig. 8). In the case of multiple-solute Mg alloys, the elements with diameter larger than Mg (i.e., Ca, RE), and the elements with diameter less than Mg (i.e., Al, Zn), are prone to co-segregate towards the GBs and dislocations. And the grain refinement efficiency would also be increased. For example, the recrystallized grain size of an extruded Mg-1Al-1Ca-0.3Zn-0.4Mn alloy can be reduced to only ~ 0.4 μm, since the Ca, Al and Zn atoms can co-segregate at GBs, enhancing the thermal stability of GBs [150]. Sun et al. showed that, the recrystallized grain size of Mg-8.2Gd-3.2Y-1.0Zn-0.4Zr alloy after HPT treatment can be even refined to only ~ 35 nm, mainly due to co-segregations of Gd, Y and Zn atoms [151,152]. The results above shown that solute segregations are effective in refining the DRX grain size in Mg alloys.

More interesting, Hucheng Pan's group found that the grain refinement in Mg alloys can be achieved via tuning the dislocation behavior, i.e., changing the dominant slipping mode from basal/prismatic <a> to the pyramidal $<c+a>$ type. In fact, it is noted that the CRSS values of different slip systems in the Mg alloys can be significantly changed after the appropriate addition of solute atoms dissolved into the Mg matrix. Especially, the addition of Ca and/or RE elements will significantly increase the basal slip CRSS value and reduce the pyramidal/basal slip CRSS ratio, which leads to an alteration in the proportion of dislocations generated in the Mg alloy, such as an increase in the proportion of $<c+a>$ dislocations. For example, Yu et al. [153] reported that due to the Y and Ca additions, Mg-5Y-0.08Ca alloy present a profound increase in CRSS for <a> basal slipping (29 ± 5 MPa), thus leading to a reduced pyramidal/basal slip CRSS ratio of ~ 7.14, as compared with the high ratio of ~ 100 for pure Mg. The simulation results also showed that the small amount of Ce addition can significantly increase the CRSS values for the basal and prismatic slipping, while it has little effect on the CRSS value for the pyramidal II slipping [154]. In this sense, Li et al. [155] prepared the model Mg-0.3Ce binary alloy and clarify the critical role of Ce addition in tuning the recrystallization behavior. It was shown that Ce addition can effectively increase the activation ratio of $<c+a>$ dislocations. Screw-typed pyramidal $<c+a>$ dislocations participate in the formation of low angle interfaces being perpendicular to the basal plane, while subsequent $<c+a>$ edge-type dislocations take part in the formation of low angle interfaces being parallel to the basal plane, ultimately leading to the formation of fine DRX grains. Because of the addition of Ce element, the dislocation component in the formed LAGBs mainly belong to the $<c+a>$ type, which exhibit much lower mobility than that of the <a> type in conventional Mg alloys. Consequently, the recrystallization temperature of the Mg-Ce alloy was increased and the recrystallization process was suppressed. Statistics show that the recrystallization grain size of the alloy is only ~ 0.5 μm (Fig. 9). The concept of

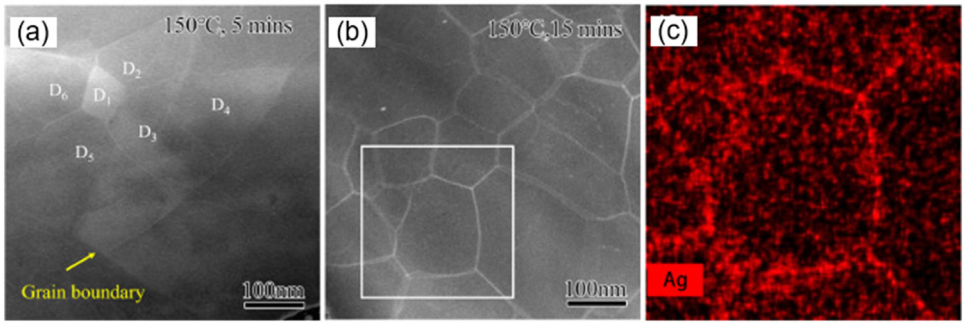

Fig. 8. HAADF-STEM images of Mg-Ag alloy [145].

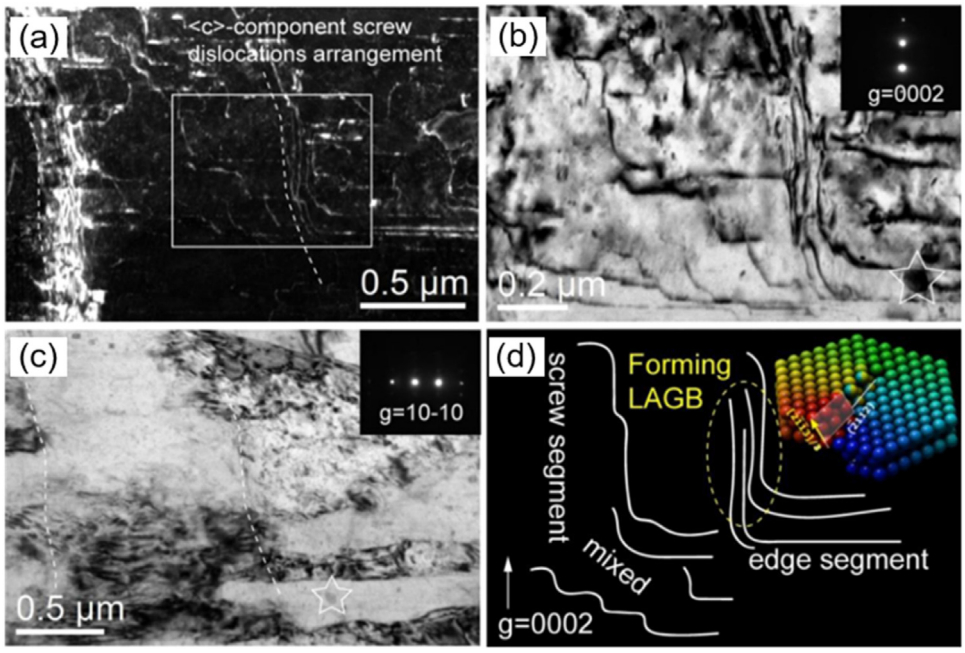

Fig. 9. Typical TEM images at the position of 7.5 mm below extrusion die exit of Mg-0.3Ce billet (a, b, c) showing the initial formation stage of LAGBs which are perpendicular to basal plane via $<c + a>$ dislocations accumulation, under the two-beam conditions of (a, b) $g = 0002$ and (c) $g = 10\bar{1}0$, and (d) the corresponding schematic image [155].

changing the CRSS for different slip systems by Ca and/or RE additions to modify the dominant deformation behavior in polycrystal and thus tune the recrystallization mechanism has also been successfully applied to the other Mg wrought alloys, including the Mg-Ce-Al [156], Mg-Ce-Ca-Al [157] and Mg-Ca-Mn-Ce [158] alloys. Generally, the average size of DRX grains formed via GBIN mechanism in Mg alloys can be as fine as < 0.5 μm, which should be effective in enhancing the yield strength.

4. High-strength wrought mg alloys based on the grain refinement strategy

4.1. Light rare-earth containing mg alloys

4.1.1. Mg-Ce-based alloys

Mg-Ce-based alloy is the typical wrought Mg alloys, and its strengthening contribution mainly come from grain refinement, rather than age-hardening, due to a quite low solid solubility in Mg. Zhao et al. [159] prepared the fine-grained Mg-Ce alloys by hot-extrusion and found that increasing Ce content leads to an obvious grain refinement effect, with the grain size of ~ 2.5 μm and ~ 2.2 μm in Mg-0.5Ce and Mg-1Ce alloys, respectively. Thus, a higher YS of ~ 295 MPa and ~ 316 MPa was obtained in extruded Mg-0.5Ce and Mg-1Ce alloys, as compared to low strength of only ~ 80 MPa in pure Mg with the grain size of ~ 29 μm. Further, Li et al. [155] optimized the extrusion process and achieved a maximum YS of ~ 356 MPa in a dilute Mg-0.3Ce alloy. They found that decreasing extrusion temperature from 350 °C to 280 °C results in a reduction of the recrystallized grain size from ~ 1.26 μm to ~ 0.51 μm, which contributes to enhanced YS values. In addition, it was shown that the extruded Mg-0.3Ce alloy characterizes the typical sub-grain lamellae with the thickness of ~ 100 nm, in which the Ce-induced multiple slipping and Ce-enriched nano-phases are

mainly responsible to the formation of sub-grain lamellae. Considering that it is difficult for further refining grain in Mg-Ce alloy by extrusion process, Pan et al. [156] employed trace Al (∼ 0.05%) addition into Mg-0.2Ce alloy to induce solute segregation at both GBs and dislocations, which thus results in the formation of ultrafine sub-grains with the size of ∼ 390 nm and ∼ 640 nm after the indirect extrusion at 260 °C and 300 °C, respectively. The highest yield strength of ∼ 365 MPa was obtained in a dilute Mg-0.2Ce-0.05Al extrusion alloy. As mentioned above, the efficient grain refinement of Mg-Ce-based alloy should be related with the reduced pyramidal/basal slip CRSS ratio due to the Ce addition [154,155,160], and more thermally stable LAGBs containing the $<c + a>$ dislocations can be formed.

4.1.2. Mg-Nd-based alloys

Mg-Nd-based (Mg-Nd-Zn-Zr) alloys have great potential for industrial applications, particularly in the biodegradable implant materials. Since Nd possess a large solid solution in the Mg matrix of ∼ 3.6 wt.% at eutectic temperature, the certain precipitation hardening by ageing is expected in Mg-Nd-based alloys. However, for the Mg-Nd-based cast alloys, the yield strength is usually lower than ∼ 200 MPa due to the large grain size (∼ 50 μm), which largely limited their extensive applications. Therefore, the grain refinement by thermomechanical processing is necessary for enhancing the strength. For example, Zheng et al. [161] refined the grain size from 25 ∼ 35 μm in as-cast sample to 10 ∼ 20 μm in the extruded Mg-3.0Nd-0.2Zn-0.4Zr (NZ30) alloy via employing hot extrusion, which also exhibit a higher yield strength of 250 ∼ 270 MPa and larger ductility of 14 ∼ 16%, comparted to coarse-grained Mg cast alloy with yield strength of ∼ 112 MPa and ductility of ∼ 12%. Zhang et al. [162] reported that increasing the extrusion ratio from 8 to 18 can significantly refined recrystallized grains of Mg-3.08Nd-0.27Zn-0.46Zr alloys extruded at 280 °C, leasing to a distinct improvement in the yield strength from ∼ 306 MPa to ∼ 360 MPa, but the ductility is slightly reduced. When the extrusion ratio is further increased to 25, the yield strength is yet decreased to ∼ 246 MPa, while the elongation greatly increases to ∼ 26.5%. This is largely because the larger extrusion ratio of 25 induces fully recrystallized fine grain structure, while the smaller extrusion ratio of 8 and 18 produce inhomogeneous grain structures consisting of fine recrystallized grains and coarse non-recrystallized grains. The inhomogeneous grain structures not only cause fine-grained hardening but also texture strengthening, which is thus favorable to the enhanced strength. Wang et al. [163] fabricated fine-grained (∼ 1 μm) Mg-2.5Nd-0.5Zn-0.5Zr sheet via using the high strain rate hot-rolling process, in which refinement strengthening, dislocation strengthening, precipitation strengthening and texture strengthening are together responsible with the high strength of 248 ∼ 298 MPa. It is suggested that the grain refinement of Mg-Nd-based alloys should be related to the PSN mechanism during the recrystallization procedure due to low solubility and high adding amount of Nd element. Besides, tuning CRSS of different slip/twin systems and also the solute segregation at grain boundaries also play the important roles [163].

4.1.3. Mg-Sm-based alloys

Among all light RE elements, Sm has the largest miscibility gap in Mg matrix (∼ 5.8% at eutectic temperature), and thereby Mg-Sm-based alloys have more obvious precipitation hardening effect than the other light-RE containing Mg alloys [164]. Similar to Mg-Nd-based cast alloys, however, Mg-Sm-based cast alloys with coarse grains often exhibit low yield strength (< 200 MPa). Likewise, refining grains via thermomechanical processing is feasible approach for the development of high-strength Mg-Sm-based alloys. Guan et al. [165] developed a high-strength Mg-3.5Sm-0.6Zn-0.5Zr alloy extruded at 320 °C, in which the yield strength of as-extruded Mg sample is as high as ∼ 363 MPa, and can further increase to 416 MPa after ageing at 200 °C for 24 h The alloy features the bimodal microstructure including ultrafine recrystallized grains with size of ∼ 470 nm and coarse unrecrystallized grains containing profuse dynamic precipitates, and thus the dominant strengthening mechanisms should be the grain-boundary hardening and dispersion strengthening. Zhang et al. [166] further optimized extrusion process and alloying composition of Mg-Sm-based alloy, and fabricated an ultrahigh-strength Mg-4Sm-0.6Zn-0.4Zr alloy, exhibiting an ultra-high yield strength of ∼ 458 MPa by low-temperature extrusion at 300 °C together with ageing at 200 °C for 28 h This alloy presented a bimodal microstructure, and the high-density Mg_3Sm particles were dynamically precipitated along grains boundaries as well as hot-worked grains interior during extrusion, which plays a crucial role in forming fine grains and strengthening matrix. In addition, Zhang et al. [167] also developed a high-strength Mg-3.5Sm-2Yb-0.6Zn-0.4Zr extruded at 300 °C, and the alloy exhibited a high yield strength of ∼ 450 MPa but a low elongation of ∼5%. Submicron recrystallized grains of 0.82 μm was obtained mainly due to the dynamic precipitation of Mg_3RE phases at grain boundaries, and thus the grain-boundary hardening contribution to the yield strength is over 120 MPa. Meanwhile, strong texture and numerous precipitated particles also contribute to the high strength. Although these Mg-Sm-Zn-Zr alloys exhibited high tensile yield strength over 400 MPa by conventional extrusion followed by artificial aging, their compression-tension yield asymmetry (CYS/TYS) is yet noticeable, with the CYS/TYS ratio of around 0.7. Therefore, further works to improve the yield asymmetry is indispensable for boarding their application. Recently, Zhang et al. [168] fabricated a low-alloyed Mg-2Sm-0.8Mn-0.6Ca-0.5Zn alloy by low-temperature and low-speed extrusion. The as-extruded alloy can exhibit an ultra-high yield strength of 453 MPa, mostly because of the fine-grained structure containing high-density residual dislocations and Mn nanoparticles. Unexpectedly, subsequent simple annealing leads to an excellent combination of high-strength of 403 MPa and high-ductility and 15.5%. Grain boundary co-segregation of Sm, Zn and Ca atoms inhibits grain growth during annealing, which is crucial to maintain high strength. This work shows the importance of

grain boundary segregation in forming fine grains to achieve both high strength and high ductility. It is thus concluded that the refined grains in Mg-Sm-based alloy are originated from both the multiple slipping system in Mg matrix due to the Sm addition, as well as the stabilized grain boundaries due to the solute segregations.

4.2. Rare earth free Mg alloys

4.2.1. Mg-Al-based alloys

Mg-Al-based alloy is the most widely used Mg alloy, especially Mg-Al-Zn (AZ) and Mg-Al-Mn (AM) series. Traditional AZ series Mg alloys lack effective grain refinement and precipitation strengthening effect, and thus the yield strength is lower than 250 MPa. Kim et al. [169] found that artificial cooling of Mg-3Al-1Zn alloy during the indirectly extrusion at low temperature could refine the grain from 5.5 μm to 1.8 μm, and yield strength at room temperature was increased ∼ 50 MPa. Li et al. [170] carried out pre-homogenization and ECAP pre-processing in AZ91 alloy before single-pass high-reduction rolling, which contributes to the improvement of formability, provides favorable conditions for further dynamic recrystallization, and also promotes the formation of bimodal microstructure, leading to the yield strength and elongation at room temperature of 335 MPa and 19 %, respectively. Razavi et al. [85] found that the texture and grain size of Mg-3Al-1Zn alloy can be accurately controlled by multi-temperature ECAP. The grain size can be refined to 0.35 μm, and excellent strength and ductility are obtained at room temperature, with the yield strength and elongation of 385 MPa and 12.7%, respectively. Zeng et al. [82] constructed ultra-fine recrystallized grains (∼ 0.65 μm) and grain boundary segregation of Zn atoms in AZ31 alloy, and found that it could significantly inhibit common intergranular deformation modes in Mg alloys, such as grain boundary sliding, grain boundary migration and grain rotation, and the yield strength of the alloy could reach 380 MPa. Yu et al. [171] prepared an ultra-high strength Mg-8Al-0.5Zn alloy via low temperature and low speed extrusion, with the yield strength of 403 MPa, the tensile strength of 437 MPa, and the elongation of 10.7%, and the tension-compression yield asymmetry was up to 0.97, which was significantly higher than traditional extrusion alloy, and the ultra-fine recrystallized grain (∼ 0.4 μm) is responsible to the excellent mechanical properties. Kim et al. [172] prepared an ultra-high strength Mg-3Al-1Zn alloy sheet with grain size of ∼ 0.6 μm by optimizing the high-ratio differential speed rolling process, where the yield strength and ultimate tensile strength at room temperature of the alloy could be enhanced to ∼ 382 MPa, and its tensile strength was 401 MPa. Zhang et al. [173] prepared a large-sized commercial AZ80 sample with dimensions of 100 × 100 × 140 mm by multi-directional forging, and the recrystallized grains could be refined to ∼ 1.5 μm, leading to a high yield strength of ∼ 343 MPa at room temperature, where the high-density defects introduced by the MDF process include grain boundaries, dislocations and stacking faults (SFs) could accelerate the subsequent aging response.

At the same time, the synergistic effect of multiple components also has an important effect on grain refinement in Mg-Al-based alloy [174]. Pan et al. [37] prepared a low-cost and high-strength Mg-Al-Ca-Zn-Mn-Ce alloy through single-pass large-strain rolling process. The nano-precipitates and solute segregation in the microstructure can effectively hinder the growth of recrystallized grains, with the size of ∼ 0.8 μm, leading to the yield strength at room temperature of ∼ 290 MPa. Fu et al. [157] found that adding a trace amount of Ce to Mg-Al-Ca alloy can induce solute segregation along dislocations and grain boundaries, widen the processing temperature range of the alloy, and obtain ultra-fine recrystallized grains with 0.7 ∼ 0.8 μm in a wide temperature range, leading to the yield strength and elongation of ∼350 MPa and 12.1%, respectively. Zha et al. [175] obtained high strength and ductility in Mg-1.1Al-1.1Zn-0.2Sn-0.3Ca alloy by sub-solidification followed by hot rolling and annealing process, and the yield strength and elongation at room temperature are ∼ 249 MPa and ∼ 14%, respectively, where the contribution of fine recrystallized grains (∼ 2 μm) and high density LAGBs to yield strength can reach ∼ 65%. Liu et al. [176] prepared a low-alloyed Mg-0.68Al-0.32Ca-0.50Mn alloy with high strength by conventional extrusion process, where the average size of DRX grains was only ∼ 2.1 μm, and the yield strength at room temperature could reach ∼ 316 MPa. The recrystallization mechanism in Mg-Al-based alloy is mainly involved GBIN and DTIN, and the poor segregation ability of Al in Mg alloys results in restricted refinement capability. Thus the refinement capacity of Mg-Al based alloys exhibit an upper limit of a few micrometers, which are produced by the conventional processing techniques (e.g. extrusion, rolling).

4.2.2. Mg-Zn-based alloys

Grain growth is easy to occur in Mg-Zn based alloy due to the low eutectic temperature, and thus the mechanical properties of low-alloyed Mg-Zn alloy are usually poor. In order to improve the strength of the alloy at room temperature, it is necessary to add trace elements such as Zr, Mn and Ca to refine the grain. Hofstetter et al. [177] prepared a low-alloyed Mg-Zn-Ca alloy with excellent mechanical properties through industrial extrusion, where the recrystallization and grain growth can be controlled by adjusting the size and distribution of the second phases, and the grain size can be refined to 1.8 μm, leading to the yield strength and elongation of 240 MPa and 30%, respectively. Zareian et al. [178] investigated the effects of Ca addition amounts on the microstructure and mechanical properties of extruded Mg-2Zn alloys, and found that when Ca content exceeded 1 wt.%, the grain refining effect was no longer obvious, and thus the size of DRX grains and yield strength at room temperature were 1.83 μm and 283 MPa in Mg-2Zn-1Ca alloy. Zhang et al. [179] found that the grain size of Mg-1Zn-0.5Ca alloy can be refined to 0.5 ∼ 0.6 μm by reducing the extrusion temperature, and the yield strength could be increased to ∼ 297 MPa. Peng et al. [180] studied the role of Mn particles in Mg-Zn alloy on its microstructure and mechanical properties, and found that the pre-existing nano-scale α-Mn particles present excellent

pinning effect on refining grains, while the micron scaled α-Mn phase can activate the PSN mechanism and promote the nucleation of recrystallized grains, which lead to the grain refinement to ~ 1.3 μm, and the yield strength and elongation at room temperature of 267 MPa and 28.6%, respectively. Jiang et al. [181] developed a low-cost high-strength Mg-0.21Zn-0.30Ca-0.14Mn alloy with yield strength and elongation of 307 MPa and 20.6%, respectively, where the bimodal structure composed of fine dynamic recrystallized grains (~ 2.3 μm) and coarse un-recrystallized grains with strong texture is the main reason. Nie et al. [182] also obtained bimodal microstructure in Mg-Zn-Ca-Mn alloys by low temperature and low speed extrusion, and the yield strength at room temperature could reach ~ 364 MPa. Du et al. [183] found that the grain size of Mg-4.50Zn-1.13Ca alloy could be significantly refined through the secondary extrusion process, and the yield strength of the low-temperature extrusion sample can reach as high as ~ 370 MPa. It is supposed that Mg-Zn alloys have weaker refining capacity due to low melting point of Mg-Zn phases and weak tuning effect of CRSS values. Formation of Mg-Zn nano-phases and the possible Zn segregations along GBs work together and lead to the certain grain refinement in Mg-Zn based wrought alloys.

4.2.3. Mg-Ca-based alloys

Mg-Ca-based alloy is a new type of high-strength Mg alloy, which has the advantages of low cost, low density and excellent biocompatibility, and has a wide range of application prospects in industrial and biomedical fields. Naoko et al. [184] studied the effect of extrusion temperature on the microstructure and mechanical properties of Mg-0.3 at.% Ca alloy, and found that the average grain size of the alloy can be refined to ~ 0.5 μm when extruded at 250 °C, and the yield strength at room temperature is ~ 363 MPa. Pan et al. [185] performed traditional one-step extrusion on Mg-1Ca to obtain multi-scale substructures, including ultrafine recrystallized grains, dispersed Mg_2Ca nano-phases and high-density residual dislocations, with yield strength up to ~ 377 MPa. Based on process optimization, Pan et al. [186] further developed an ultra-high strength Mg-1Ca alloy, where the DRX grains can be refined to 0.2 ~ 0.5 μm, and the yield strength at room temperature can be increased to ~ 377 MPa. She et al. [187] found that the addition of Mn element can help to hinder the grain growth during the extrusion process of Mg-Ca alloy, thus increasing the yield strength of the alloy by ~ 120 MPa. Liu et al. [188] prepared Mg-0.3Ca alloy with excellent mechanical properties by low temperature extrusion, where the yield strength and elongation at room temperature were 361 MPa and 10.6%, respectively, mainly due to the segregation of Ca atoms at grain boundaries, which refined the DRX grains to ~ 0.7 μm. Pan et al. [95] found a controllable strategy for developing Mg-Ca-Al-Zn-Mn alloy with excellent mechanical properties, and the bimodal microstructure with ultra-fine recrystallized grains (~ 0.33 μm) and low residual dislocation was constructed by optimizing the extrusion temperature, which provided excellent grain refinement hardening effect, where the yield strength and elongation at room temperature reached ~ 425 MPa and ~ 11%, respectively. Mg-Ca based alloys have many similar effects with Mg-RE based alloys, suggesting that the Ca atom can act as the alternative element to develop high performance RE-free Mg alloys [153,189,190]. It has been reported that the Ca can dramatically tailor both the CRSS values and segregation energy [190]. Moreover, the strong tendency of interaction between Ca and Al/Zn [144] give more space to manipulate the microstructure of Mg-Ca alloys. The refinement pathways of Mg-Ca based alloys include promoting $<c + a>$ dislocations percentage via reducing pyramidal/basal CRSS ratio, promoting multi-element segregation at grain boundaries/dislocations, as well as facilitating nano-precipitations to pin the grain boundaries.

4.2.4. Mg-Sn-based alloys

Compared with Mg-Al-based and Mg-Zn-based alloys, Mg-Sn-based alloys can be extruded over a wider range of extrusion temperatures and speeds. Zhou et al. [191] found that ECAP method can significantly refine the grain size of Mg-Sn-Zn-Zr alloy, and promote non-basal slip and texture weakening, where the yield strength and elongation at room temperature were ~ 311 MPa and ~ 20.5%, respectively. A novel dilute Mg-0.5Sn-0.7Al-0.8Zn alloy was developed by Cheng and directly extruded after casting process, and the grain size of ~ 1.79 μm and the yield strength of ~ 262 MPa were achieved [192]. Elsayed et al. [193] developed a new type Mg-Sn-Al-Zn-Na alloy through low temperature and low speed extrusion with the average grain size of ~ 0.4 μm and the yield strength of ~336 MPa. Otherwise, Yan et al. [194] found that low temperature extrusion in Mg-3Sn-2Al-1Zn alloy can effectively refine the average size of DRX grains to ~ 0.46 μm, and an ultra-high yield strength of ~ 413 MPa was achieved. Pan et al. [195] found that adding 1 wt.% Ca element to Mg-2Sn can refine the DRX grain size to ~ 0.8 μm, and promote the formation of high-density dislocations, sub-grain boundaries and nano-phases, contributing to the yield strength of ~ 269 MPa. Subsequently, a new low-alloyed high-strength Mg-2Sn-2Ca alloy was developed by conventional extrusion process, and the yield strength at room temperature reached ~ 443 MPa, where the ultra-fine grain (~ 0.32 μm) was the main reason for its excellent mechanical properties. The characteristics of low content of alloying elements, fast extrusion process and low cost make it extremely potential for large-scale industrial applications [148]. Based on this, Zhang et al. [149] further developed low-alloyed Mg-2.0Sn-1.95Ca-0.5Mn alloy, which increased the yield strength to ~450 MPa at room temperature. The Sn element exhibits an appreciable solubility in Mg alloy, which sharply decrease with decreasing temperature [196]. Thus PSN mechanism would be included in the high-alloyed Mg-Sn based samples containing numerous second phases. For convenience, Fig. 10 summarized the Hall-Petch relationship for the RE-free Mg alloys above, including the Mg-Al based, Mg-Zn based, Mg-Ca based and Mg-Sn based alloys. It can be seen that the ultra-high strength above 450 MPa has been achieved in RE-free Mg alloys mainly due to the effec-

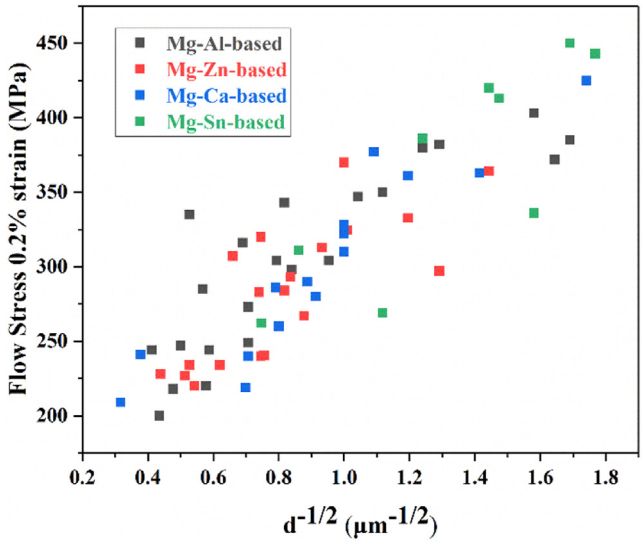

Fig. 10. Plot of yield stress vs. $d^{-1/2}$ of different alloys systems.

tive grain refinement, which should be comparable with other high-content RE elements containing Mg wrought alloys.

4.3. Grain refinement strengthening efficiency of different alloy system

The grain refining strengthening strategy in Mg alloys is more effective than that in Al alloys as mentioned above. However, the k value of Hall-Petch relationship has a large variation in different systems. Basically, the main factors that affect k values include CRSS of different slip systems, solute segregation, coherency of the grain boundary, temperature, and so on. Importantly, the texture is one major factor that dramatically influence the k value [197,198] (Fig. 11). Different alloying element contribute to the large difference in texture, which thus results in an obvious variation in the k values. For example, Wen et al. [81]. compared the k value of extruded Mg-0.35at.%X alloy (X represents Y, Gd, Al, Zn), and found that Mg-Y/Gd alloys exhibit the low k values of 220∼285 MPa·μm$^{1/2}$, while Mg-Al/Zn alloys present higher k value of ∼ 323 MPa·μm$^{1/2}$. The weakened texture is usually formed in the Gd/Y-containing Mg alloys, which lead to the activation of easy mode of <a> slipping, which thus contribute to the low k value. Jing et al. [199]. obtained the similar low k value of ∼ 280 in Mg-1Gd-2Zn alloy. In contrast, the k value of a hot-rolled AZ31 plate can be increased up to 411 MPa·μm$^{1/2}$ since the non-basal slipping becomes the dominant mode. Beside slipping, deformation by twining can also lead to the large discrepancy in the k values, ranging from 219 MPa·μm$^{1/2}$ to 435 MPa·μm$^{1/2}$ [200]. It is speculated that the different activation stress for twinning between the two neighboring grains should be major reason. Moreover, it is noted the k values mentioned above are calculated in the grain size range of more than 1 μm. When the grain size is refined down to sub-micrometer scale (650 nm for instance), the dominant deformation mode would transit to the grain boundary sliding [201,202], which resulted in the reversed Hall-Petch relationship. Nevertheless, when decreasing the deformation temperature to cryogenic temperature [203] or using the grain boundary segregation strategy [152,204], the ordinary Hall-Petch relationship would re-establish, and the critical grain size for reversed Hall-Petch relationship can be further decreased.

5. Perspectives and outstanding issues

Mg alloys naturally present low density and high specific strength, thus having unique competitive advantage as structural material in terms of lightweight applications. However, traditional strengthening approaches such as solid solution strengthening and precipitate strengthening in Mg alloys cannot be comparable with those in Al alloys and steel. Fortunately, polycrystalline Mg alloys usually present higher Hall-Petch slope than that of the counterpart Al alloys, which is mostly associated with the low ability of intergranular deformation due to the limited number of slipping systems. Consequently, the yield strength can reach as high as 300 ∼ 350 MPa in Mg alloy, when the grain size is decreased to only the sub-micrometer scale. In other words, grain refinement is the most effective way for strengthening in Mg wrought alloys, especially for the low-alloyed Mg alloys. In the following, we would give two scientific and engineering issues that are hitherto important in this field.

The first issue is to develop low-cost and heat-resistant Mg alloy *via* constructing fine grained structure with excellent thermal stability. It is proposed that promoting multiple slip system during plastic deformation can be a promising strategy to fabrication ultrafine grained alloys with strong texture, and also the high density of LAGBs with low-energy character can be formed via controlling the recrystallization process. On the one hand, the constructed dislocation walls are thermally stable and the migration resistant is high, due to the $<c + a>$-type character with relatively larger CRSS values. On the other hand, the formed LAGBs exhibit a high lattice coherency, and the relaxed grain boundaries can be stable against migration under thermal activation, which has been verified in other metals, including Al, Cu and Ni alloys. Moreover, solute segregation at grain boundaries can dramatically reduce the grain boundary energy and make these boundaries become more stable. In this context, the possible case of solute precipitations at GBs at high temperature should be avoided. Rational design of grain boundary segregation can be achieved via optimizing the solute elements with high segregation energy and low diffusion coefficient in Mg alloys. It will be useful in the future work for fabricating the ultrafine grained alloys with both high thermal stability and high temperature mechanical property.

The second issue is to explore the extreme value for grain refinement in Mg alloys prepared by the traditional fabrication process. The importance of multiple slip system in grain refinement has been verified in the typical Mg-Ce based alloy. However, the role the other ternary element on grain refine-

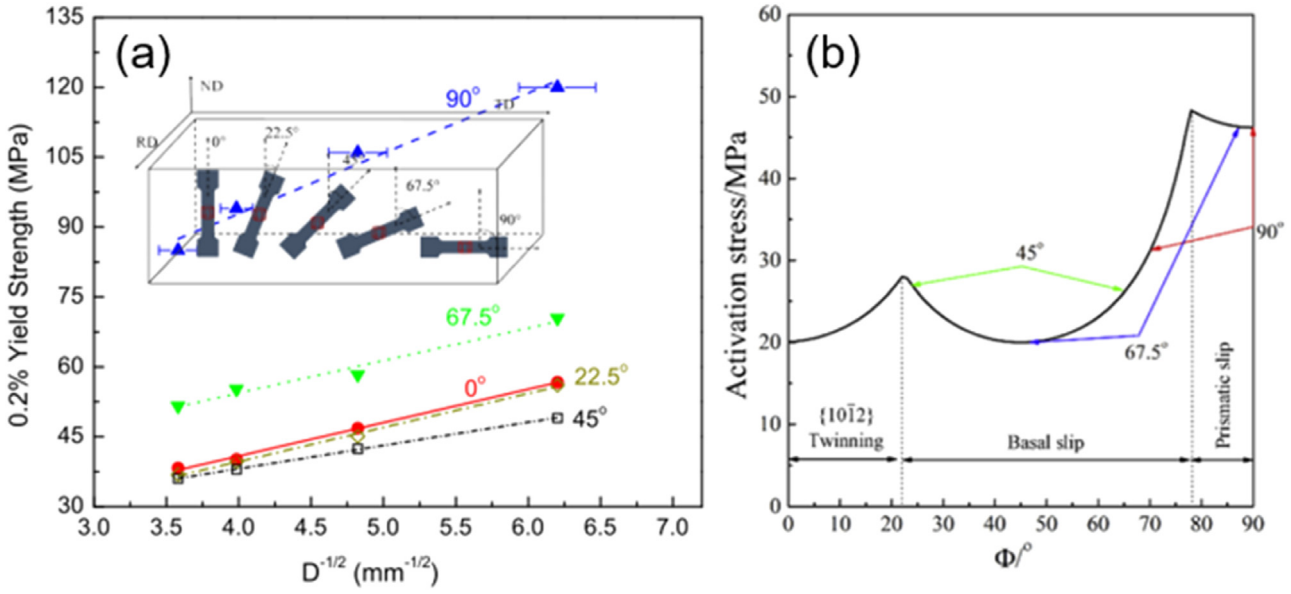

Fig. 11. Hall-Petch relations affected by texture. (a) k values established as a function of tension tilting angle from the ND and (b) the related mechanism based on activation stress for initiated deformation mode as a function of tilting angle of the c-axis away from direction of tension [197,198].

ment of Mg-Ce based alloys, and the development of other Mg based alloys, should be emphasized in the future. Specifically, the CRSS values variation in the ternary and multiple Mg alloying systems above should be clarified, and the dislocation activation, movement and rearrangement in the newly developed Mg alloy should be investigated, with the purpose of achieving more effective grain refinement and thus the high strength in Mg alloys. More interestingly, when the homogeneous CRSS value among different slip system is realized in Mg alloys, the strength-ductility combination can be also expected. In this sense, we propose a new designing concept for Mg wrought alloys, namely the strategy of solid solution strengthening and plasticization, to achieve both grain refinement during fabrication and high strength-ductility synergy during post tension.

Declaration of competing interest

The authors declare that they have no known competing financial interests or personal relationships that could have appeared to influence the work reported in this paper.

CRediT authorship contribution statement

Sen Wang: Data curation, Writing – original draft. **Hucheng Pan:** Funding acquisition, Supervision, Writing – original draft, Writing – review & editing. **Dongsheng Xie:** Data curation, Investigation. **Dongdong Zhang:** Data curation, Investigation. **Jingren Li:** Data curation, Investigation, Methodology, Writing – original draft, Writing – review & editing. **Hongbo Xie:** Data curation, Investigation. **Yuping Ren:** Conceptualization, Supervision. **Gaowu Qin:** Funding acquisition, Supervision, Writing – review & editing.

Acknowledgments

This work was supported by National Key Research and Development Program of China (No. 2023YFB3710900), National Natural Science Foundation of China (Nos. U2241235, U2167213, 51971053), and funded by the Project of Promoting Talents in Liaoning province (No. XLYC2203202). H.C. Pan acknowledges the financial assistance from Young Elite Scientists Sponsorship Program by CAST (20192021QNRC001, 2019–2021QNRC002, 2019–2021QNRC003), and the fund from the Fundamental Research Funds for the Central Universities (N2202020).

References

[1] J. Song, J. Chen, X. Xiong, X. Peng, D. Chen, F. Pan, J. Magnes. Alloy. 10 (4) (2022) 863–898.
[2] J.F. Nie, K.S. Shin, Z.R. Zeng, Metall. Mater. Trans. A 51 (12) (2020) 6045–6109.
[3] Z. Zeng, M. Zhou, M. Esmaily, Y. Zhu, S. Choudhary, J.C. Griffith, J. Ma, Y. Hora, Y. Chen, A. Gullino, Q. Shi, H. Fujii, N. Birbilis, Commun. Mater. 3 (1) (2022) Article 18.
[4] Y. Yang, X. Xiong, J. Chen, X. Peng, D. Chen, F. Pan, J. Magnes. Alloy. 9 (3) (2021) 705–747.
[5] J. Ni, L. Jin, J. Zeng, J. Li, F. Wang, F. Wang, S. Dong, J. Dong, J. Magnes. Alloy. 11 (1) (2023) 1–14.
[6] G.G. Wang, J.P. Weiler, J. Magnes. Alloy. 11 (1) (2023) 78–87.
[7] Z.Z. Jin, M. Zha, S.Q. Wang, S.C. Wang, C. Wang, H.L. Jia, H.Y. Wang, J. Magnes. Alloy. 10 (5) (2022) 1191–1206.
[8] R.G. Li, Y. Yan, H.C. Pan, H. Zhang, J.R. Li, G.W. Qin, B.S. Liu, Mater. Res. Lett. 10 (10) (2022) 682–689.
[9] X. Wei, L. Jin, F. Wang, J. Li, N. Ye, Z. Zhang, J. Dong, J. Mater. Sci. Technol. 44 (2020) 19–23.
[10] D. Zhang, H. Pan, Z. Zeng, W. Tang, J. Li, H. Xie, R. Li, Y. Ren, G. Qin, J. Magnes. Alloy. (2023).
[11] P. Peng, J. She, Q. Yang, S. Long, A. Tang, J. Zhang, Q. Dai, F. Pan, J. Alloy. Compd. 935 (2023) Article 168008.

[12] X. Ma, M. Zha, S. Wang, Y. Yang, H. Jia, D. Gao, C. Wang, H. Wang, J. Magnes. Alloy. 10 (10) (2022) 2889–2900.
[13] L. Li, C. Zhang, H. Lv, C. Liu, Z. Wen, J. Jiang, J. Magnes. Alloy. 10 (1) (2022) 249–265.
[14] M. Maleki, S. Berndorf, S. Mohammadzehi, H. Mirzadeh, M. Emamy, M. Ullmann, U. Prahl, J. Alloy. Compd. 954 (2023) Article 170224.
[15] R.G. Li, H.R. Li, H.C. Pan, D.S. Xie, J.H. Zhang, D.Q. Fang, Y.Q. Dai, D.Y. Zhao, H. Zhang, Scr. Mater. 193 (2021) 142–146.
[16] Z. Zhang, X. Liu, Z. Wang, Q. Le, W. Hu, L. Bao, J. Cui, Mater. Design. 88 (2015) 915–923.
[17] X. Luo, Z. Feng, T. Yu, J. Luo, T. Huang, G. Wu, N. Hansen, X. Huang, Acta Mater. 183 (2020) 398–407.
[18] A. Lakshmanan, M.T. Andani, M. Yaghoobi, J. Allison, A. Misra, V. Sundararaghavan, J. Magnes. Alloy. (2023).
[19] Y. Kawamura, K. Hayashi, A. Inoue, T. Masumoto, Mater. Trans. 42 (7) (2001) 1172–1176.
[20] C. Sun, H. Liu, Z. Xu, Y. Wu, K. Yan, J. Ju, J. Jiang, F. Xue, J. Bai, Y. Xin, J. Mater. Sci. Technol. 176 (2024) 13–24.
[21] T. Homma, N. Kunito, S. Kamado, Scr. Mater. 61 (6) (2009) 644–647.
[22] J. Xie, Z. Zhang, S. Liu, J. Zhang, J. Wang, Y. He, L. Lu, Y. Jiao, R. Wu, Int. J. Miner. Metall. Mater. 30 (1) (2023) 82–91.
[23] R.G. Li, J.F. Nie, G.J. Huang, Y.C. Xin, Q. Liu, Scr. Mater. 64 (10) (2011) 950–953.
[24] W.W. Jian, G.M. Cheng, W.Z. Xu, H. Yuan, M.H. Tsai, Q.D. Wang, C.C. Koch, Y.T. Zhu, S.N. Mathaudhu, Mater. Res. Lett. 1 (2) (2013) 61–66.
[25] S.K. Panigrahi, W. Yuan, R.S. Mishra, R. DeLorme, B. Davis, R.A. Howell, K. Cho, Mater. Sci. Eng. A 530 (2011) 28–35.
[26] X. Zheng, W. Du, Z. Wang, S. Li, K. Liu, X. Du, Mater. Lett. 212 (2018) 155–158.
[27] A.E. Davis, J.D. Robson, M. Turski, Acta Mater. 158 (2018) 1–12.
[28] T.T. Sasaki, F.R. Elsayed, T. Nakata, T. Ohkubo, S. Kamado, K. Hono, Acta Mater. 99 (2015) 176–186.
[29] Z.Y. Chen, Q. Zhang, Q.A. Li, H.X. Zhu, X.Y. Chen, X.Y. Li, P.J. Chen, J. Bao, J. Mater. Res. Technol. 15 (2021) 5582–5596.
[30] K. Liu, S.C. Zhao, C.L. Wang, L.P. Wang, Y.C. Feng, D.R. Liu, J.F. Li, Z.W. Wang, Materials 14 (19) (2021) 5667 Article 5667.
[31] R. Shi, J. Miao, T. Avey, A.A. Luo, Sci. Rep. 10 (1) (2020) Article 10044.
[32] T. Nakata, C. Xu, R. Ajima, K. Shimizu, S. Hanaki, T.T. Sasaki, L. Ma, K. Hono, S. Kamado, Acta Mater. 130 (2017) 261–270.
[33] X. Zheng, J. Dong, D. Yin, W. Liu, F. Wang, L. Jin, W. Ding, Mater. Sci. Eng. A 527 (16) (2010) 3690–3694.
[34] Z. Zhang, J. Zhang, J. Xie, S. Liu, Y. He, R. Wang, D. Fang, W. Fu, Y. Jiao, R. Wu, Mater. Sci. Eng. A 831 (2022) Article 142259.
[35] M. Kavyani, G.R. Ebrahimi, H.R. Ezatpour, M. Jahazi, J. Magnes. Alloy. 10 (6) (2022) 1640–1662.
[36] S. Wang, F.H. Gao, B.J. Lv, N. Cui, F. Guo, J. Mater. Eng. Perform. 32 (6) (2023) 2635–2645.
[37] H. Pan, R. Cheng, S. Du, H. Xie, L. Wu, Z. Deng, C. Yang, L. Ma, G. Qin, J. Mater. Eng. Perform. 29 (11) (2020) 7115–7124.
[38] C.L. Mendis, J.H. Bae, N.J. Kim, K. Hono, Scr. Mater. 64 (4) (2011) 335–338.
[39] G. Hu, D. Zhang, T. Tang, X. Shen, L. Jiang, J. Xu, F. Pan, Mater. Sci. Eng. A 634 (2015) 5–13.
[40] X.Q. Liu, X.G. Qiao, R.S. Pei, Y.Q. Chi, L. Yuan, M.Y. Zheng, J. Magnes. Alloy. 11 (2) (2023) 553–561.
[41] X.R. Zhuo, C. Shao, P. Zhang, Z.C. Hu, H. Liu, Metals 12 (8) (2022) Article 1341.
[42] H. Wu, J. Jiang, Z. Yang, M. Li, H. Huang, N. Ge, A. Ma, H. Liu, J. Magnes. Alloy. (2022).
[43] Z. Gui, F. Wang, J. Zhang, D. Chen, Z. Kang, J. Magnes. Alloy. 10 (1) (2022) 239–248.
[44] S.A. Torbati-Sarraf, R. Mahmudi, Mater. Sci. Eng. A 527 (15) (2010) 3515–3520.
[45] H. Miura, X. Yang, T. Sakai, Mater. Trans. 49 (2008) 1015–1020.
[46] J. Li, F. Wang, J. Zeng, C. Zhao, C. Qian, F. Wang, S. Dong, L. Jin, J. Dong, J. Magnes. Alloy. (2022).
[47] C. Cui, W. Zhang, W. Chen, J. He, X. Chen, J. Hou, J. Magnes. Alloy. 10 (10) (2022) 2745–2760.
[48] M.M. Hoseini-Athar, R. Mahmudi, R.P. Babu, P. Hedstrom, Mater. Sci. Eng. A 808 (2021) Article 140921.
[49] W. Sun, Y. He, X. Qiao, X. Zhao, H. Chen, N. Gao, M.J. Starink, M. Zheng, J. Magnes. Alloy. (2022).
[50] S.X. Ding, W.T. Lee, C.P. Chang, L.W. Chang, P.W. Kao, Scr. Mater. 59 (9) (2008) 1006–1009.
[51] W. Li, X. Liu, Y. Zheng, W. Wang, W. Qiao, K.W.K. Yeung, K.M.C. Cheung, S. Guan, O.B. Kulyasova, R.Z. Valiev, Biomater. Sci. 8 (18) (2020) 5071–5087.
[52] A.H. Feng, Z.Y. Ma, Scr. Mater. 56 (5) (2007) 397–400.
[53] F.Y. Liu, R.L. Xin, C.P. Wang, B. Song, Q. Liu, Scr. Mater. 158 (2019) 131–135.
[54] P. Vignesh, G. Venkatesh, S. Kumaran, J. Mater. Eng. Perform. 31 (7) (2022) 5288–5297.
[55] C.Y. Ma, X.F. Guan, L. Sun, G.J. Liu, Mater. Sci. Eng. A 831 (2022) Article 142278.
[56] J. Zhang, Q. Ma, F. Pan, Mater. Design. 31 (9) (2010) 4043–4049.
[57] Y.H. Kim, H.T. Sohn, W.J. Kim, Mater. Sci. Eng. A 597 (2014) 157–163.
[58] T. Bhattacharjee, T. Nakata, T.T. Sasaki, S. Kamado, K. Hono, Scr. Mater. 90-91 (2014) 37–40.
[59] W. Fu, P. Dang, S. Guo, Z. Ren, D. Fang, X. Ding, J. Sun, J. Mater. Sci. Technol. 134 (2023) 67–80.
[60] J. Wang, P. Song, S. Huang, F. Pan, Mater. Lett. 93 (2013) 415–418.
[61] S. Zhang, W. Liu, X. Gu, C. Lu, G. Yuan, W. Ding, J. Alloy. Compd. 557 (2013) 91–97.
[62] X. Jin, W. Xu, D. Shan, B. Guo, B.C. Jin, Mater. Design. 199 (2021) Article 109384.
[63] N. Su, Y. Wu, Q. Deng, Z. Chang, Q. Wu, Y. Xue, K. Yang, Q. Chen, L. Peng, Mater. Sci. Eng. A 810 (2021) Article 141019.
[64] X. Liu, D. Huang, C. Yan, Y. Zhou, W. Yan, Mater. Charact. 167 (2020) Article 110511.
[65] J. Zuo, L. Hou, J. Shi, H. Cui, L. Zhuang, J. Zhang, J. Alloy. Compd. 708 (2017) 1131–1140.
[66] M.H. Goodarzy, H. Arabi, M.A. Boutorabi, S.H. Seyedein, S.H. Hasani Najafabadi, J. Alloy. Compd. 585 (2014) 753–759.
[67] R. Alizadeh, J. Llorca, Acta Mater. 186 (2020) 475–486.
[68] Z.H. Huang, C.M. Yang, L. Qi, J.E. Allison, A. Misra, Mater. Sci. Eng. A 742 (2019) 278–286.
[69] J.J. Bhattacharyya, F. Wang, N. Stanford, S.R. Agnew, Acta Mater. 146 (2018) 55–62.
[70] X.H. Shao, Q.Q. Jin, Y.T. Zhou, H.J. Yang, S.J. Zheng, B. Zhang, Q. Chen, X.L. Ma, Mater. Sci. Eng. A 779 (2020) Article 139109.
[71] C.Y. Wang, C.M. Cepeda-Jimenez, M.T. Perez-Prado, Acta Mater. 194 (2020) 190–206.
[72] G. Esteban-Manzanares, A.X. Ma, I. Papadimitriou, E. Martinez, J. Llorca, Model. Simul. Mater. *Sc*. 27 (7) (2019) Article 075003.
[73] B.J. Zhou, L.Y. Wang, G.M. Zhu, J. Wang, W. Wen, X.Q. Zeng, JOM 70 (10) (2018) 2315–2320.
[74] M. Liao, B. Li, M.F. Horstemeyer, Metall. Mater. Trans. A 45A (8) (2014) 3661–3669.
[75] Z. Savaedi, H. Mirzadeh, R.M. Aghdam, R. Mahmudi, J. Mater. Res. Technol. 19 (2022) 3100–3109.
[76] Z. Savaedi, H. Mirzadeh, R.M. Aghdam, R. Mahmudi, Mater. Today Commun. 33 (2022) Article 104825.
[77] A. Koushki, A. Heydarinia, M. Emamy, H. Mirzadeh, M.S. Mehranpour, Mater. Sci. Technol. 38 (17) (2022) 1434–1438.
[78] H. Somekawa, T. Mukai, Mater. Sci. Eng. A 561 (2013) 378–385.
[79] N. Hansen, Acta Mater. 25 (8) (1977) 863–869.
[80] T. Huang, L. Shuai, A. Wakeel, G. Wu, N. Hansen, X. Huang, Acta Mater. 156 (2018) 369–378.
[81] Y. Wen, B. Guan, Y. Xin, C. Liu, P. Wu, G. Huang, Q. Liu, Scr. Mater. 210 (2022) Article 114451.
[82] Z.R. Zeng, Y.M. Zhu, R.L. Liu, S.W. Xu, C.H.J. Davies, J.F. Nie, N. Birbilis, Acta Mater. 160 (2018) 97–108.
[83] H.S. Kim, Y. Estrin, M.B. Bush, Acta Mater. 48 (2) (2000) 493–504.

[84] Z. Li, C. Hou, M. Huang, C. Ouyang, Comput. Mater. Sci. 46 (4) (2009) 1124–1134.
[85] S.M. Razavi, D.C. Foley, I. Karaman, K.T. Hartwig, O. Duygulu, L.J. Kecskes, S.N. Mathaudhu, V.H. Hammond, Scr. Mater. 67 (5) (2012) 439–442.
[86] Z. Zhang, J.-h. Zhang, J. Wang, Z.-h. Li, J.-s. Xie, S.-j. Liu, K. Guan, R.-z. Wu, Int. J. Miner. Metall. Mater. 28 (1) (2021) 30–45.
[87] J. Lin, W. Ren, Q. Wang, L. Ma, Y. Chen, Adv. Mater. Sci. Eng. 2014 (2014) Article 356572.
[88] X.P. Luo, D.Q. Fang, Y.S. Chai, B. Yang, Microsc. Res. Tech. 79 (8) (2016) 707–711.
[89] X.W. Liu, L.P. Bian, F. Tian, S.J. Han, T. Wang, W. Liang, Mater. Charact. 188 (2022) Article 111910.
[90] F.G. Qi, D.F. Zhang, X.H. Zhang, X.X. Xu, Mater. Sci. Eng. A 593 (2014) 70–78.
[91] Z.R. Zeng, M.Z. Bian, S.W. Xu, C.H.J. Davies, N. Birbilis, J.F. Nie, Scr. Mater. 108 (2015) 6–10.
[92] Z. Ding, G. Zhao, H. Sun, S. Li, F. Ma, E.J. Lavernia, Y. Zhu, W. Liu, J. Phys. Condens. Matter. 32 (1) (2019) Article 015401.
[93] M.M. Hoseini-Athar, R. Mahmudi, R.P. Babu, P. Hedström, J. Alloy. Compd. 831 (2020) Article 154766.
[94] H.K. Lin, J.C. Huang, T.G. Langdon, Mater. Sci. Eng. A 402 (1) (2005) 250–257.
[95] H. Pan, R. Kang, J. Li, H. Xie, Z. Zeng, Q. Huang, C. Yang, Y. Ren, G. Qin, Acta Mater. 186 (2020) 278–290.
[96] X. Ye, Z. Suo, Z. Heng, B. Chen, Q. Wei, J. Umeda, K. Kondoh, J. Shen, J. Magnes. Alloy. (2023).
[97] C. Zheng, S. Chen, M. Cheng, S. Zhang, Y. Li, Y. Yang, J. Magnes. Alloy. (2023).
[98] H. Mirzadeh, J. Mater. Res. Technol. 25 (2023) 7050–7077.
[99] H. Conrad, W.D. Robertson, Trans. Am. Ins. Min. Metall. Eng. 209 (4) (1957) 503–512.
[100] J.W. Cha, S.H. Park, J. Magnes. Alloy. (2022).
[101] C.M. Sellars, W.J. Mctegart, Acta Mater. 14 (9) (1966) 1136–1138.
[102] L. Hu, M. Lang, L. Shi, M. Li, T. Zhou, C. Bao, M. Yang, J. Magnes. Alloy. 11 (3) (2023) 1016–1028.
[103] X. Chen, Q. Liao, Y. Niu, W. Jia, Q. Le, C. Cheng, F. Yu, J. Cui, J. Mater. Res. Technol. 8 (2) (2019) 1859–1869.
[104] X. Shen, D. Zhang, C. Yao, L. Tan, X. Li, Mater. Today Commun. 31 (2022) 103772.
[105] D.C. Ludwigson, Metall. Trans. 2 (10) (1971) 2825–2828.
[106] E. Voce, J. Ins. Met. 74 (1948) 537–562.
[107] H. Mecking, U.F. Kocks, Acta Mater. 29 (11) (1981) 1865–1875.
[108] Y. Estrin, H. Braasch, Y. Brechet, J. Eng. Mater. Technol. 118 (4) (1996) 441–447.
[109] A. Laasraoui, J.J. Jonas, Metall. Trans. A 22 (7) (1991) 1545–1558.
[110] H.W. Swift, J. Mech. Phys. Solids 1 (1) (1952) 1–18.
[111] M.H. Barezban, R. Roumina, H. Mirzadeh, R. Mahmudi, Met. Mater. Int. 27 (5) (2021) 843–850.
[112] L. Li, Y. Wang, H. Li, W. Jiang, T. Wang, C.C. Zhang, F. Wang, H. Garmestani, Comput. Mater. Sci. 166 (2019) 221–229.
[113] M. Avrami, J. Chem. Phys. 9 (2) (2004) 177–184.
[114] K. Kumar, N. Ansari, R.L. Narayan, J. Jain, J. Alloy. Compd. 955 (2023) Article 170329.
[115] S.H. Choi, D.H. Kim, H.W. Lee, E.J. Shin, Mater. Sci. Eng. A 527 (4) (2010) 1151–1159.
[116] Y. Cai, C.Y. Sun, Y.L. Li, S.Y. Hu, N.Y. Zhu, E.I. Barker, L.Y. Qian, Int. J. Plast. 133 (2020) Article 102773.
[117] Y. Song, M. Wang, Y. Zong, R. He, J. Jin, Materials 11 (10) (2018) Article 1903.
[118] N.Y. Zhu, C.Y. Sun, Y.L. Li, L.Y. Qian, S.Y. Hu, Y. Cai, Y.H. Feng, Comput. Mater. Sci. 200 (2021) 110858.
[119] E. Popova, Y. Staraselski, A. Brahme, R.K. Mishra, K. Inal, Int. J. Plast. 66 (2015) 85–102.
[120] X. Duan, M. Wang, X. Che, L. He, J. Liu, J. Mater. Sci. 58 (3) (2023) 1345–1367.
[121] Y. He, IOP Conf. Ser. Earth Environ. Sci. 742 (1) (2021) Article 012004.
[122] M. Mohseni, A.R. Eivani, H. Vafaeenezhad, H.R. Jafarian, M.T. Salehi, J. Zhou, J. Mater. Res. Technol. 15 (2021) 3585–3597.
[123] E.A. Ball, P.B. Prangnell, Scr. Mater. 31 (2) (1994) 111–116.
[124] S.W. Xu, N. Matsumoto, S. Kamado, T. Honma, Y. Kojima, Scr. Mater. 61 (3) (2009) 249–252.
[125] S.W. Xu, S. Kamado, N. Matsumoto, T. Honma, Y. Kojima, Mater. Sci. Eng. A 527 (1–2) (2009) 52–60.
[126] X. Xia, K. Zhang, X. Li, M. Ma, Y. Li, Mater. Des. 44 (2013) 521–527.
[127] T. Al-Samman, Mater. Sci. Eng. A 560 (2013) 561–566.
[128] R. Pei, S. Korte-Kerzel, T. Al-Samman, Materialia 12 (2020) Article 100715.
[129] J.D. Robson, D.T. Henry, B. Davis, Acta Mater. 57 (9) (2009) 2739–2747.
[130] F.J. Humphreys, H. M, Recrystallization and Related Annealing Phenomena, Elsevier, 2012.
[131] X. Li, P. Yang, L.N. Wang, L. Meng, F. Cui, Mater. Sci. Eng. A 517 (1–2) (2009) 160–169.
[132] I. Basu, T. Al-Samman, Acta Mater. 96 (2015) 111–132.
[133] D.K. Guan, W.M. Rainforth, L. Ma, B. Wynne, J.H. Gao, Acta Mater. 126 (2017) 132–144.
[134] J. Hjelen, R. Ørsund, E. Nes, Acta Mater. 39 (7) (1991) 1377–1404.
[135] Z.R. Zeng, Y.M. Zhu, S.W. Xu, M.Z. Bian, C.H.J. Davies, N. Birbilis, J.F. Nie, Acta Mater. 105 (2016) 479–494.
[136] N. Stanford, M.R. Barnett, Mater. Sci. Eng. A 496 (1) (2008) 399–408.
[137] D. Guan, W.M. Rainforth, J. Gao, L. Ma, B. Wynne, Acta Mater. 145 (2018) 399–412.
[138] M.G. Jiang, C. Xu, H. Yan, G.H. Fan, T. Nakata, C.S. Lao, R.S. Chen, S. Kamado, E.H. Han, B.H. Lu, Acta Mater. 157 (2018) 53–71.
[139] A. Imandoust, C.D. Barrett, A.L. Oppedal, W.R. Whittington, Y. Paudel, H. El Kadiri, Acta Mater. 138 (2017) 27–41.
[140] A. Imandoust, C.D. Barrett, T. Al-Samman, M.A. Tschopp, E. Essadiqi, N. Hort, H. El Kadiri, Metall. Mater. Trans. A 49 (5) (2018) 1809–1829.
[141] C.D. Barrett, A. Imandoust, A.L. Oppedal, K. Inal, M.A. Tschopp, H. El Kadiri, Acta Mater. 128 (2017) 270–283.
[142] C.D. Barrett, A. Imandoust, H. El Kadiri, Scr. Mater. 146 (2018) 46–50.
[143] J.D. Robson, Metall. Mater. Trans. A 45a (8) (2014) 3205–3212.
[144] R. Pei, Y. Zou, D. Wei, T. Al-Samman, Acta Mater. 208 (2021) Article 116749.
[145] L.R. Xiao, X.F. Chen, Y. Cao, H. Zhou, X.L. Ma, D.D. Yin, B. Ye, X.D. Han, Y.T. Zhu, Scr. Mater. 177 (2020) 69–73.
[146] J. Zhang, Y. Dou, Y. Zheng, Scr. Mater. 80 (2014) 17–20.
[147] Z. Zhang, J. Zhang, J. Xie, S. Liu, W. Fu, R. Wu, Int. J. Plast. 162 (2023) Article 103548.
[148] H. Pan, G. Qin, Y. Huang, Y. Ren, X. Sha, X. Han, Z.Q. Liu, C. Li, X. Wu, H. Chen, C. He, L. Chai, Y. Wang, J.F. Nie, Acta Mater. 149 (2018) 350–363.
[149] A. Zhang, R. Kang, L. Wu, H. Pan, H. Xie, Q. Huang, Y. Liu, Z. Ai, L. Ma, Y. Ren, G. Qin, Mater. Sci. Eng. A 754 (2019) 269–274.
[150] M. Li, D. Xie, J. Li, H. Xie, Q. Huang, H. Pan, G. Qin, Mater. Charact. 175 (2021) Article 111049.
[151] W.T. Sun, X.G. Qiao, M.Y. Zheng, C. Xu, S. Kamado, X.J. Zhao, H.W. Chen, N. Gao, M.J. Starink, Acta Mater. 151 (2018) 260–270.
[152] W.T. Sun, X.G. Qiao, M.Y. Zheng, X.J. Zhao, H.W. Chen, N. Gao, M.J. Starink, Scr. Mater. 155 (2018) 21–25.
[153] M. Yu, Y. Cui, J. Wang, Y. Chen, Z. Ding, T. Ying, J. Llorca, X. Zeng, Int. J. Plast. 162 (2023) Article 103525.
[154] J.K. Lee, B.J. Lee, Metall. Mater. Trans. A 52 (3) (2021) 964–974.
[155] J.R. Li, D.S. Xie, Z.R. Zeng, B. Song, H.B. Xie, R.S. Pei, H.C. Pan, Y.P. Ren, G.W. Qin, J. Mater. Sci. Technol. 132 (2023) 1–17.
[156] H. Pan, D. Xie, J. Li, H. Xie, Q. Huang, Q. Yang, G. Qin, Mater. Res. Lett. 9 (8) (2021) 329–335.
[157] T. Fu, X. Sun, C. Ge, D. Xie, J. Li, H. Pan, G. Qin, J. Alloy. Compd. 917 (2022) Article 165407.
[158] X. Sun, C. Ge, C. Yang, D. Zhang, J. Li, D. Xie, H. Pan, G. Qin, Mater. Charact. 188 (2022) Article 111922.

[159] D. Zhao, G. Li, P. Li, J. Zhou, K. Cheng, Y. Liu, Y. Yang, J. Duan, R. Ghomashchi, X. Wang, Mater. Sci. Eng. A 803 (2021) Article 140508.
[160] J. Ye, R.K. Mishra, A.K. Sachdev, A.M. Minor, Scr. Mater. 64 (3) (2011) 292–295.
[161] X. Zheng, J. Dong, Y. Xiang, J. Chang, F. Wang, L. Jin, Y. Wang, W. Ding, Mater. Des. 31 (3) (2010) 1417–1422.
[162] X.B. Zhang, G.Y. Yuan, Z.Z. Wang, Mater. Sci. Technol. 29 (1) (2013) 111–116.
[163] S. Wang, W. Zhang, H. Wang, J. Yang, W. Chen, G. Cui, G. Wang, Mater. Sci. Eng. A 803 (2021) Article 140488.
[164] K. Guan, C. Li, Z. Yang, Y. Yu, Q. Yang, W. Zhang, Z. Guan, C. Wang, M. Zha, H. Wang, J. Magnes. Alloy. (2023).
[165] K. Guan, Q. Yang, F. Bu, X. Qiu, W. Sun, D. Zhang, T. Zheng, X. Niu, X. Liu, J. Meng, Mater. Sci. Eng. A 703 (2017) 97–107.
[166] D. Zhang, H. Pan, J. Li, D. Xie, D. Zhang, C. Che, J. Meng, G. Qin, Mater. Sci. Eng. A 833 (2022) Article 142565.
[167] D. Zhang, Q. Yang, K. Guan, B. Li, N. Wang, P. Qin, B. Jiang, C. Sun, X. Qin, Z. Tian, Z. Cao, J. Meng, J. Alloy. Compd. 810 (2019) Article 151967.
[168] Z. Zhang, J. Zhang, J. Xie, S. Liu, Y. He, K. Guan, R. Wu, Scr. Mater. 209 (2022) Article 114414.
[169] B. Kim, C.H. Park, H.S. Kim, B.S. You, S.S. Park, Scr. Mater. 76 (2014) 21–24.
[170] Y. Li, Y. Jiang, Q. Xu, A. Ma, J. Jiang, H. Liu, Y. Yuan, C. Qiu, Mater. Sci. Eng. A 804 (2021) Article 140717.
[171] H. Yu, S.H. Park, B.S. You, Mater. Sci. Eng. A 610 (2014) 445–449.
[172] W.J. Kim, Y.G. Lee, M.J. Lee, J.Y. Wang, Y.B. Park, Scr. Mater. 65 (12) (2011) 1105–1108.
[173] Z. Zhang, L. Yuan, M. Zheng, Q. Wei, D. Shan, B. Guo, J. Mater. Process. Technol. 311 (2023) Article 117828.
[174] J. Zhang, P. Peng, Q. Yang, A.A. Luo, J. Magnes. Alloy. (2023).
[175] M. Zha, S.C. Wang, H.L. Jia, Y. Yang, P.K. Ma, H.Y. Wang, Mater. Sci. Eng. A 862 (2023) Article 144457.
[176] X. Liu, X. Qiao, Z. Li, M. Zheng, Mater. Charact. 162 (2020) Article 110197.
[177] J. Hofstetter, S. Rüedi, I. Baumgartner, H. Kilian, B. Mingler, E. Povoden-Karadeniz, S. Pogatscher, P.J. Uggowitzer, J.F. Löffler, Acta Mater. 98 (2015) 423–432.
[178] Z. Zareian, M. Emamy, M. Malekan, H. Mirzadeh, W.J. Kim, A. Bahmani, Mater. Sci. Eng. A 774 (2020) Article 138929.
[179] B.P. Zhang, L. Geng, L.J. Huang, X.X. Zhang, C.C. Dong, Scr. Mater. 63 (10) (2010) 1024–1027.
[180] P. Peng, J. She, A. Tang, J. Zhang, K. Song, Q. Yang, F. Pan, J. Alloy. Compd. 890 (2022) Article 161789.
[181] M.G. Jiang, C. Xu, T. Nakata, H. Yan, R.S. Chen, S. Kamado, J. Alloy. Compd. 668 (2016) 13–21.
[182] K.B. Nie, Z.H. Zhu, P. Munroe, K.K. Deng, J.G. Han, Acta Metall. Sin. 33 (7) (2020) 922–936 (Engl. Lett.).
[183] Y.Z. Du, M.Y. Zheng, X.G. Qiao, K. Wu, X.D. Liu, G.J. Wang, X.Y. Lv, M.J. Li, X.L. Liu, Z.J. Wang, Y.T. Liu, Mater. Sci. Eng. A 583 (2013) 69–77.
[184] N. Ikeo, M. Nishioka, T. Mukai, Mater. Lett. 223 (2018) 65–68.
[185] H. Pan, G. Qin, Y. Ren, L. Wang, S. Sun, X. Meng, J. Alloy. Compd. 630 (2015) 272–276.
[186] H. Pan, C. Yang, Y. Yang, Y. Dai, D. Zhou, L. Chai, Q. Huang, Q. Yang, S. Liu, Y. Ren, G. Qin, Mater. Lett. 237 (2019) 65–68.
[187] J. She, S.B. Zhou, P. Peng, A.T. Tang, Y. Wang, H.C. Pan, C.L. Yang, F.S. Pan, Mater. Sci. Eng. A 772 (2020) Article 138796.
[188] X.Q. Liu, X.G. Qiao, W.C. Xie, R.S. Pei, L. Yuan, M.Y. Zheng, Mater. Sci. Eng. A 839 (2022) Article 142847.
[189] R. Pei, Y. Zou, M. Zubair, D. Wei, T. Al-Samman, Acta Mater. (2022) 233.
[190] J. Wang, Y. Chen, Z. Chen, J. Llorca, X. Zeng, Acta Mater. 217 (2021).
[191] T. Zhou, F. Guo, Q. Zhang, D. Liu, Mater. Lett. 305 (2021) Article 130764.
[192] W. Cheng, Y. Liu, Y. Zhang, S. Meng, S. Arthanari, H.X. Wang, L. Wang, Met. Mater. Int. 27 (11) (2021) 4510–4516.
[193] F.R. Elsayed, T.T. Sasaki, T. Ohkubo, H. Takahashi, S.W. Xu, S. Kamado, K. Hono, Mater. Sci. Eng. A 588 (2013) 318–328.
[194] X. Yan, W. Ding, W. Guo, J. Wu, H. Shu, Y. Chen, Mater. Sci. Technol. 36 (5) (2020) 575–583.
[195] H. Pan, G. Qin, M. Xu, H. Fu, Y. Ren, F. Pan, Z. Gao, C. Zhao, Q. Yang, J. She, B. Song, Mater. Des. 83 (2015) 736–744.
[196] C.L. Mendis, C.J. Bettles, M.A. Gibson, S. Gorsse, C.R. Hutchinson, Phil. Mag. Lett. 86 (7) (2006) 443–456.
[197] Y. Wang, H. Choo, Acta Mater. 81 (2014) 83–97.
[198] B. Guan, Y. Xin, X. Huang, P. Wu, Q. Liu, Acta Mater. 173 (2019) 142–152.
[199] J. Xu, B. Guan, Y. Xin, X. Wei, G. Huang, C. Liu, Q. Liu, J. Mater. Sci. Technol. 99 (2022) 251–259.
[200] H. Yu, C. Li, Y. Xin, A. Chapuis, X. Huang, Q. Liu, Acta Mater. 128 (2017) 313–326.
[201] R. Zheng, J.P. Du, S. Gao, H. Somekawa, S. Ogata, N. Tsuji, Acta Mater. 198 (2020) 35–46.
[202] Z. Zeng, M. Zhou, P. Lynch, F. Mompiou, Q. Gu, M. Esmaily, Y. Yan, Y. Qiu, S. Xu, H. Fujii, C. Davies, J.F. Nie, N. Birbilis, Acta Mater. 206 (2021) 116648.
[203] R. Zheng, W. Gong, J.P. Du, S. Gao, M. Liu, G. Li, T. Kawasaki, S. Harjo, C. Ma, S. Ogata, N. Tsuji, Acta Mater. 238 (2022).
[204] K. Bryła, J. Morgiel, M. Faryna, K. Edalati, Z. Horita, Mater. Lett. 212 (2018) 323–326.